Received: 29 July 2023 | Revised: 21 September 2023 | Accepted: 24 October 2023

DOI: 10.1002/suco.202300603

ARTICLE

fib CEB-FIP WILEY

Fatigue behavior of deep concrete beams with critical shear cracks

Eissa Fathalla[1,2] | **Boyan Mihaylov**[1]

[1]Urban and Environmental Research Unit (UEE), Univ. of Liège, Liège, Belgium

[2]Structural Engineering Department, Cairo University, Giza, Egypt

Correspondence
Eissa Fathalla, Urban and Environmental Research Unit (UEE), Univ. of Liège, Building B52, Quartier Polytech 1, Allée de la Découverte 9, B-4000 Liège, Belgium.
Email: mmeissa@uliege.be

Funding information
Service Public de Wallonie, Grant/Award Number: 2010240

Abstract

Reinforced concrete deep beams in bridges and other critical infrastructure are subjected to millions of load cycles during their service life. At the same time, they typically work with high shear and develop critical diagonal cracks. The cyclic loading across the cracks results in fatigue damage of the shear-resisting mechanisms, which needs to be taken into account in the assessment of existing structures, and in particular in members with small amount of shear reinforcement built according to early design codes. To aid the development of advanced assessment approaches for such structures, this paper presents five large-scale fatigue tests of deep beams with a stirrup ratio of 0.134%. The beams are preloaded to develop complete diagonal cracks, and then are subjected to cycles with different minimum and maximum load. The focus is placed on detailed crack measurements, needed for the development of crack-based assessment approaches. The crack data is analyzed with the help of the two-parameter kinematic theory to quantify important deformations. It is shown that the fatigue across the shear cracks is associated mainly with degradation of aggregate interlock and progressive damage in the critical loading zones. It is also shown that as the maximum load is decreased, the fatigue life increases, and the failure mode can switch from shear to flexure.

KEYWORDS

fatigue damage, pier caps, *P–N* diagram, reinforced concrete, shear-critical deep beams

1 | INTRODUCTION

Reinforced concrete (RC) deep beams with shear-span-to-effective-depth ratios $a/d \leq 2.0$ are widely used in concrete infrastructure, and most commonly in bridges. Important examples include deep girders, pier caps, and pile caps. These members are subjected to millions of load cycles during their service life, leading to high-cycle fatigue associated with deterioration of their load-resisting mechanisms. At the same time, much of the infrastructure across the world was built before the 1970s with limited design provisions for fatigue degradation.[1] At present, this infrastructure is nearing the end of its service life, while the resources for its maintenance and replacement are limited. Therefore, there is a pressing need for innovative advanced assessment methods, which can accurately evaluate the remaining service life of deep members, taking into account the effect of fatigue loading.

The fatigue flexural behavior of slender members is typically governed by fatigue fracture of the longitudinal reinforcement.[2–4] Assessment of such failures is performed based on the stress range in the reinforcement, which is evaluated using conventional sectional models. In the case of fatigue shear behavior, studies showed that slender beams mainly fail in diagonal cracking failure by

unstable crack propagation, or by fatigue fracture of the transverse reinforcement.[5–7] In one of these studies,[7] the impact of the slenderness ratio $a/d = 2.0–6.36$ on the fatigue shear strength was examined on small-scale specimens without web reinforcement. According to these experimental results, it was demonstrated that as the slenderness ratio decreases, the behavior changes from beam action to arch action and the fatigue strength starts to increase. On the other hand, in the case of deep beams ($a/d < 2.0$), the fatigue shear behavior is much more complex. The shear is carried by the compression zone near the loading plate, aggregate interlock, transverse reinforcement, and dowel action of the flexural reinforcement. Deep members can fail by inclined crushing of the compression region at the zone of loading (so-called critical loading zone, CLZ), by fatigue fracture of the stirrups, or by fatigue fracture of the longitudinal flexural reinforcement.[8–12]

An advanced crack-based assessment approach for shear-critical deep beams has been recently proposed by Trandafir et al.[13,14] for monotonic loading conditions. This approach focuses on the main indicator of damage in deep members: shear cracks which extend from the supports to the loading points of the member. Such diagonal cracks, reaching widths of up to 1 mm, have been observed in existing bridges and have raised questions about the safety of critical infrastructure.[15] In the crack-based assessment approach, the measured geometry and vertical crack displacements are used in combination with the two-parameter kinematic theory (2PKT)[16,17] to assess the residual capacity of the member. To extend this approach to capture fatigue effects, it is necessary to account for the degradation of the shear mechanisms across the critical diagonal cracks, as well as the associated widening of the cracks. However, while crack displacements are key for crack-based assessment, there is no detailed experimental data on crack displacements in fatigue tests of deep beams.

An earlier large-scale experimental program on fatigue behavior of deep beams was reported by Teng et al.[10,11] The study focused on the impact of the amount and arrangement of web reinforcement, as well as on the range of the cyclic load. It was demonstrated that the web reinforcement was effective in restraining the shear cracks and increasing the fatigue life. It was also shown that the fatigue life increases when the load range is reduced. This research focused on the global behavior of the deep beams in terms of their fatigue life without detailed measurements of crack displacements. In addition, the beams were not preloaded to develop complete diagonal cracks prior to fatigue loading, as often observed in existing bridges. Such critical cracks tend to develop early in the life of the structure, followed by a large number of load cycles applying shear across the cracks.

In this context, the current study focuses on unfavorable but realistic cases of fatigue behavior of deep beams. The test specimens feature small amount of shear reinforcement to represent existing structures built according to early design codes. In addition, all beams are initially loaded to 70% of their monotonic capacity in order to cause complete diagonal shear cracks, prior to applying fatigue cycles with various minimum and maximum loads. Detailed measurements of crack displacements are performed along the shear and flexural cracks, and they are used together with the 2PKT approach to quantify important deformations. The crack data and analysis are aimed to aid researchers in developing reliable assessment models for deep members subjected to repetitive loading.

2 | EXPERIMENTAL PROGRAM

2.1 | Test specimens

Five nominally identical deep beams with rectangular section were built for the experimental program—see Figure 1. The beams had a total length of 3200 mm, a span of 2400 mm, a total depth of 800 mm, and a width of 250 mm. The steel reinforcement consisted of 8Ø20 mm bottom longitudinal deformed bars placed in two layers, 2Ø20 mm top deformed bars, and vertical web reinforcement (stirrups) made of diameter 8 mm deformed bars with a spacing of 300 mm. The corresponding flexural reinforcement ratio ρ_l was 1.37% and the shear reinforcement ratio ρ_v was 0.134%.

2.2 | Material properties

2.2.1 | Concrete

Normal strength concrete with identical mix design was used for casting the five test specimens. Three batches of concrete were used: the first for beams P3/P4, the second for P5/P6, and the last batch for beam P7. The clear concrete cover was 25 mm and the type of coarse aggregate used was gravel with a maximum size of 22 mm. For material characterization, three compression tests were conducted per concrete batch on standard 300 mm × 150 mm cylinders. With the exception of the first batch, all cylinders were tested with strain measurements to obtain the complete pre-peak stress–strain response, including the modulus of elasticity E_c, the concrete strength f_c, and the strain at peak stress ε_{c1}. For the batch of beams

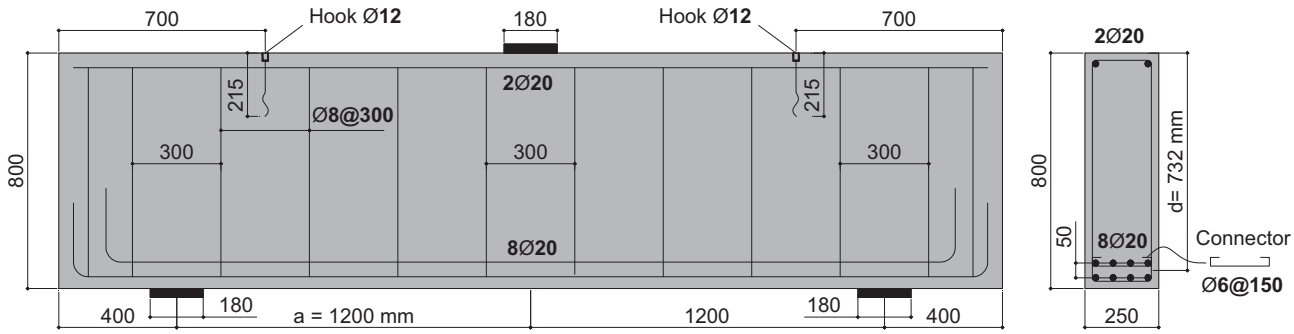

FIGURE 1 Geometry and reinforcement of test specimens.

TABLE 1 Concrete material properties of deep beams.

Beam	Compressive strength f_c' (MPa)	Strain at peak stress ε_{c1} (‰)	Modulus of elasticity E_c (MPa)	Concrete age (Days)
P3/P4	40.5	1.7	34,300	353
P5/P6	39.6	2.2	29,700	427
P7	39.7	2.4	25,800	492

P3/P4, only one cylinder was tested with strain measurements, while the other two were tested to obtain solely the concrete strength. The compressive strength obtained for all three batches was approximately 40 MPa. The main results from the cylinder tests are summarized in Table 1, while Figure 2 shows the complete pre-peak stress–strain curves of the three batches of concrete.

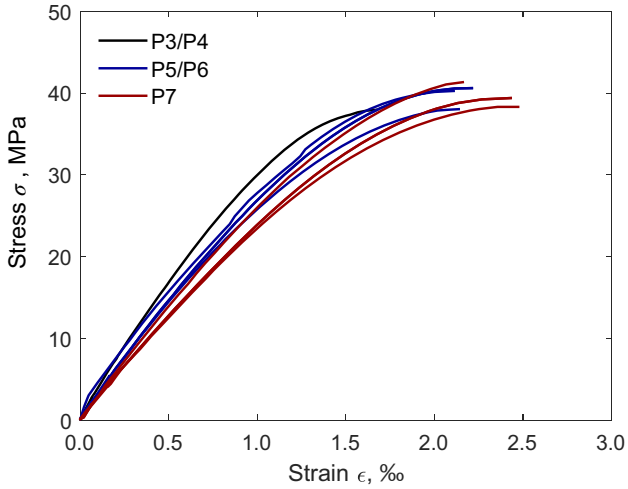

FIGURE 2 Pre-peak compression behavior of concrete.

TABLE 2 Properties of steel reinforcement.

Bar	Yield strength f_y (MPa)	Ultimate strength f_u (MPa)	Modulus of elasticity E_s (MPa)	Yield strain ε_y (‰)	Rupture strain ε_u (‰)
∅ 20	534	616	203,000	2.63	97
∅ 8	523	595	174,000	3.00	50

2.2.2 | Reinforcement

Standard tensile tests were performed on one sample of the 20 mm bars (longitudinal reinforcement) and three samples of the 8 mm bars (stirrups). The reinforcement did not exhibit a clear yield plateau and had a yield strength of approximately 530 MPa. Table 2 summarizes the main average properties obtained in the reinforcement tests.

2.3 | Test setup

Figure 3 shows the test setup used in the experimental program. The beams were tested under symmetrical 3-point bending, where the shear span was $a = 1200$ mm and the shear-span-to-effective-depth ratio a/d was 1.64 ($d = 732$ mm). The load was applied via a hydraulic jack equipped with a load cell and a spherical hinge, while the supports were rollers to ensure unrestrained elongation of the beams.

The jack load was transferred to the beam via a 180 mm × 250 mm × 30 mm steel plate. A thin layer of plaster was placed between the plate and the concrete surface to ensure uniform contact. The support reactions were applied via 180 mm × 250 mm × 30 mm steel plates. The out-of-plane stability of the beams was ensured by steel frames located at the axes of the two supports on both sides of the beam (Figure 3). To minimize the friction, Teflon pads were placed between the steel frames and the test specimen.

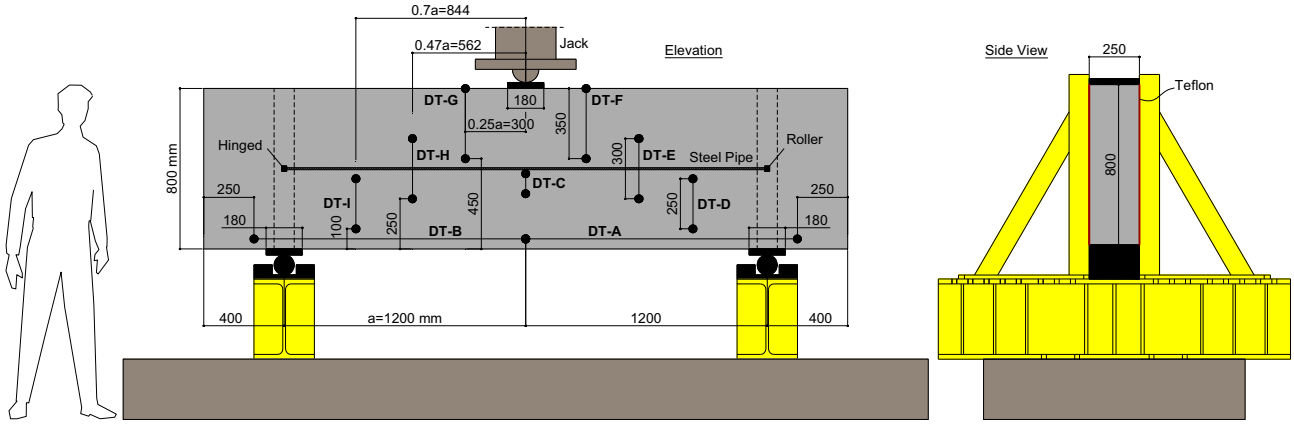

FIGURE 3 Test setup and instrumentation of deep beams. Displacement transducers DT-D and DT-I were only placed for the monotonic test P3.

2.4 | Measuring instrumentation

Figure 3 shows the instrumentation designed to measure global and local deformations for both monotonic and fatigue loading of the beams. Nine displacement transducers (DTs) were placed on one side of the beams in a symmetrical pattern across the two shear spans. Transducers DT-A and DT-B were used to measure the average strain along the bottom flexural reinforcement, and DT-C was used to measure the mid-span deflection with respect to a steel bar connected to the beam at the support axes. The remaining six transducers were placed along the expected diagonal cracks to measure the vertical displacements in the cracks: DT-F and DT-G were located at a distance of 0.25 of the shear span a measured from the center of the loading plate, DT-E and DT-H at 0.47a, and DT-D and DT-I were at 0.70a from the center of the plate. For the fatigue testing, continuous measurements were performed only with DT-C (mid-span deflection), while the other transducers were used during intermediate slow cycles within the fatigue cycles.

2.5 | Loading scheme and parameters

As mentioned earlier, one beam (P3) was tested to failure under monotonic loading to serve as a reference specimen. The applied load at failure of this beam is denoted as P_u: the monotonic ultimate capacity (strength). Beams P4, P5 and P6 were tested under fatigue loading with different maximum fatigue loads $P_{\max}$ varying from 70% to 45.1% of P_u (Table 3), while the minimum fatigue load $P_{\min}$ was kept constant at 9.7% of P_u. Beam P7 was tested similarly to beam P5 with $P_{\max} = 54.1\%$ of P_u, but with a higher minimum fatigue load $P_{\min}$ of 22.5% of P_u.

TABLE 3 Load levels of tested deep beams in fatigue.

Beam	Loading type	$P_{\max}/P_u$ %	$P_{\min}/P_u$ %	$R = P_{\min}/P_{\max}$ %
P3	Monotonic	100	-	-
P4	Fatigue	69.8	9.7	13.8
P5	Fatigue	54.7	9.7	17.6
P6	Fatigue	45.1	9.7	21.4
P7	Fatigue	54.7	22.5	41.2

In the monotonic test, the loading was initially conducted in load control (rate ~2 kN/s) in five load steps up to ~96% of the failure load. Following this load level, the control was switched to displacements (rate ~0.01 mm/s) in order to capture the post-peak response of the beam. After each load step, the load was decreased by 10% and kept constant while conducting crack width measurements and taking photos for reporting.

As mentioned in the introduction, in the fatigue tests, the beams were firstly loaded monotonically to 70% of P_u (650 kN) in order to create major diagonal shear cracks. More specifically, it was ensured that the diagonal cracks propagated from the inner edges of the support plates to the compression zone in the vicinity of the loading plate. Following this step, the fatigue loading was applied according to the load levels listed in Table 3 for each beam. The fatigue loading followed a sinusoidal wave with a frequency of 2 Hz. It is important to point out that the fatigue performance of deep beams may be impacted by the pre-cracking load in terms of initial state of stress of the shear resisting mechanisms before the application of the fatigue loading, and therefore this variable needs to be investigated further in future testing.

As mentioned earlier, continuous displacement measurements were conducted only for the mid-span deflection (transducer DT-C). For this reason, as shown in Figure 4, intermediate slow cycles were performed to connect the other displacement transducers and to perform full measurements at several intermediate stages during the fatigue loading. In the beginning of each set of intermediate slow cycles, load stages at maximum and minimum fatigue loads were conducted to measure crack widths and take photos for reporting.

3 | EXPERIMENTAL RESULTS

3.1 | Monotonic test P3

The reference beam P3 failed at a total load $P_u = 932$ kN (shear force $V_u = 466$ kN) by crushing of the concrete in the compression zone near the loading plate, accompanied by the opening of a critical diagonal crack—see Figure 5. The crushed zone was located above the critical diagonal crack, and it is referred to as the critical loading zone (CLZ).[16,17]

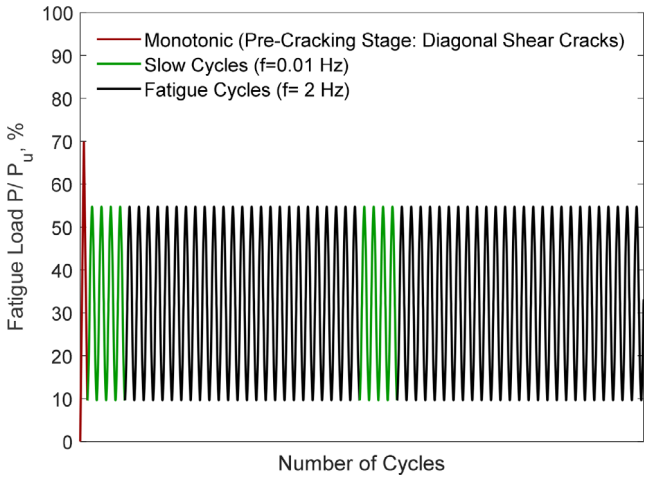

FIGURE 4 Sample loading history for fatigue tests.

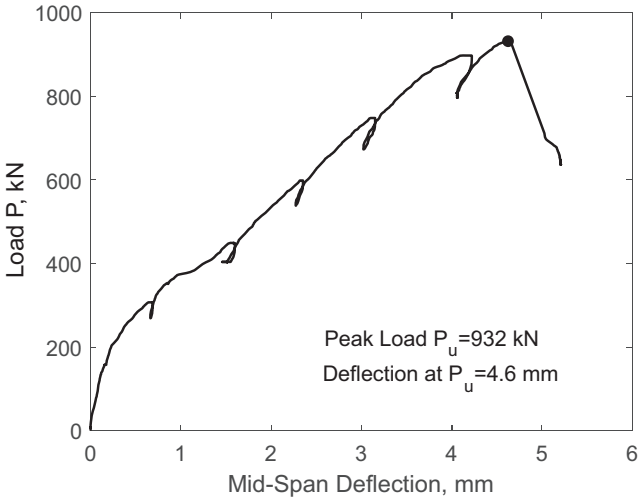

FIGURE 6 Global response—beam P3.

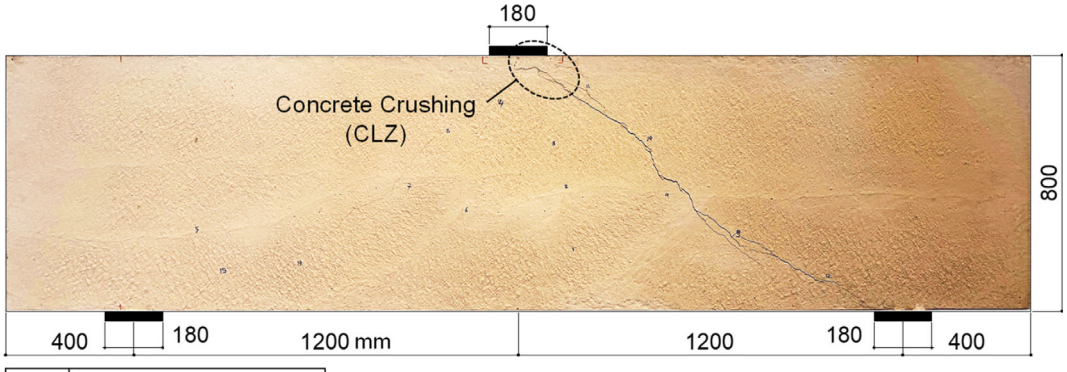

Point	Crack Width, mm Load Level P/P_u, %				
	29	43	58	72	87
1	---	0.14	0.19	0.39	0.73
2	---	0.50	0.68	1.00	1.01
3	---	0.35	0.70	0.95	1.58
4	---	0.35	0.65	0.89	1.48
5	---	0.20	0.27	0.41	0.46
6	0.09	0.23	0.30	0.30	0.31
7	0.10	0.15	0.19	0.26	0.30
8	0.09	0.13	0.13	0.14	0.17

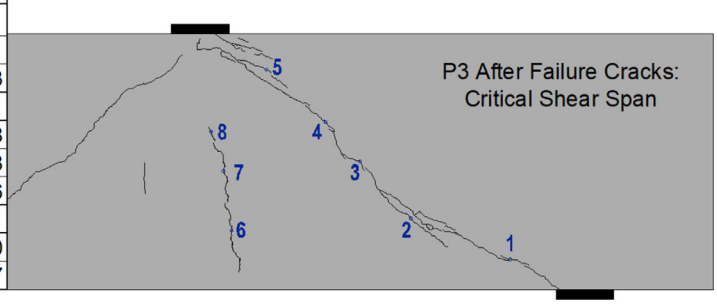

FIGURE 5 Cracks after failure (top) and crack width measurements at different load levels (bottom)—beam P3.

Figure 6 shows the global response of the beam in terms of applied load versus mid-span deflection. The specimen behaved linearly up to ~21% of the peak load

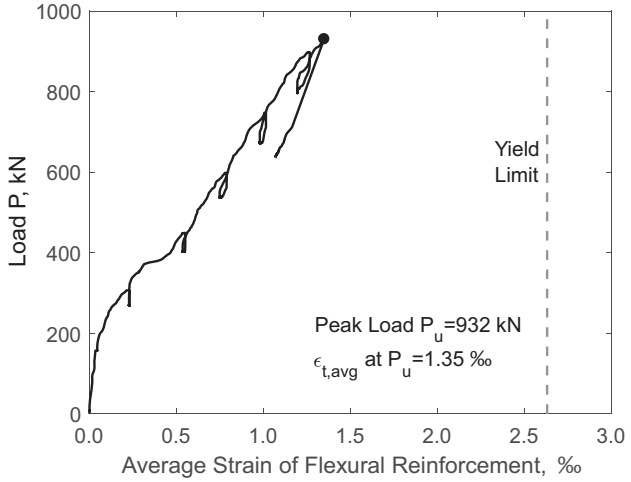

FIGURE 7 Flexural response—beam P3.

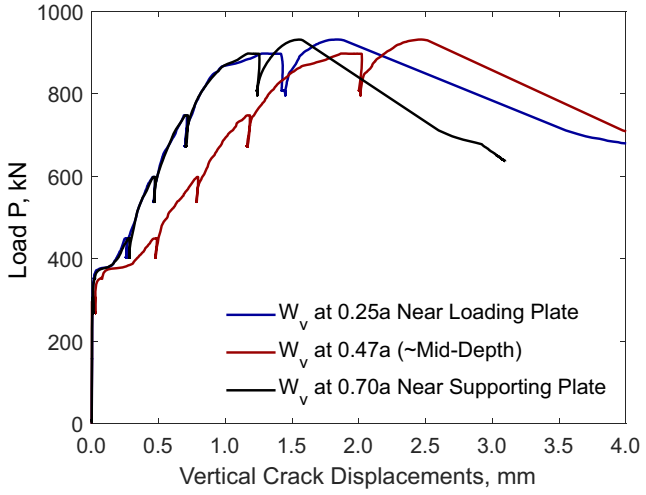

FIGURE 8 Vertical crack displacements—beam P3.

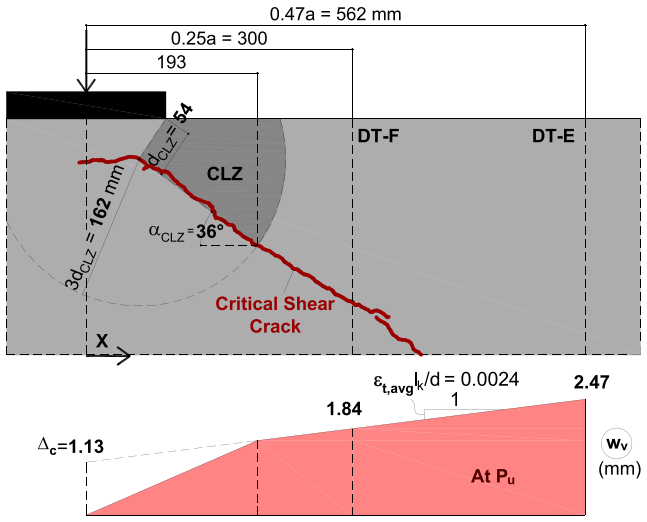

FIGURE 10 Measured geometry of CLZ and estimated DOF Δ_c of kinematic model—beam P3.

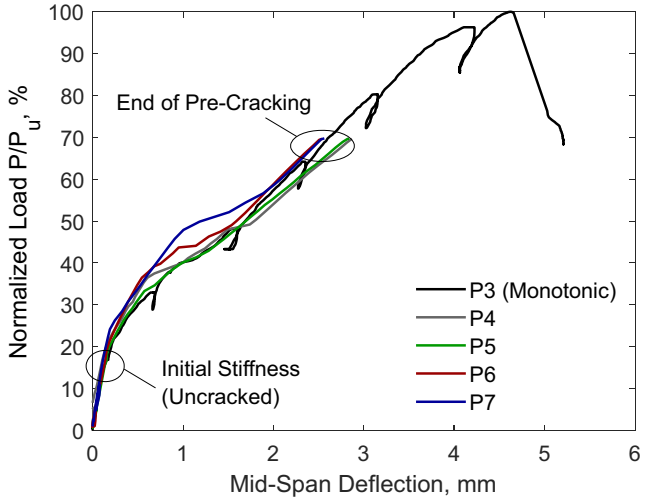

FIGURE 11 Global response of beams P4 to P7 in the pre-cracking phase, together with the complete response of beam P3 to failure.

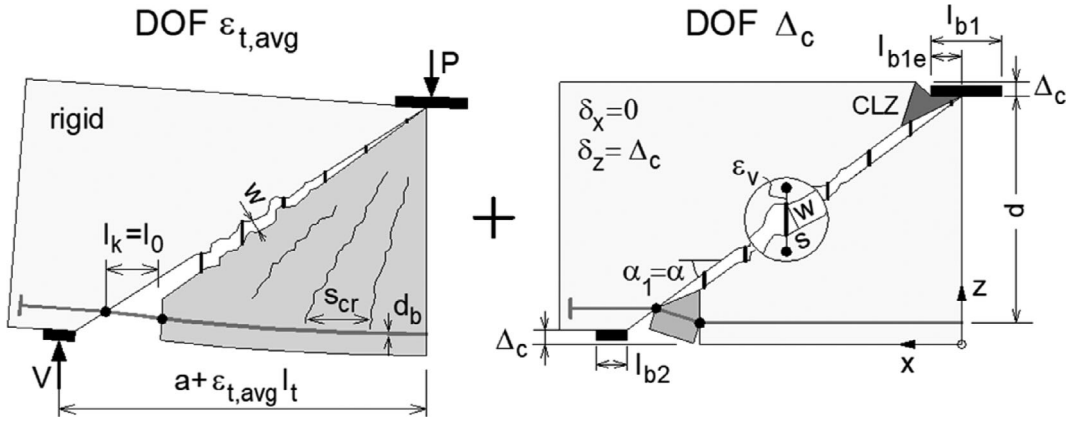

FIGURE 9 Two-parameter kinematic model for deep beams.[16,17]

(196 kN) when flexural cracks occurred in the mid-span region and the tangent stiffness decreased. With subsequent loading, the beam behaved linearly again up to ~40% of P_u (373 kN) when shear cracks propagated from the inner edges of the supports to the vicinity of the CLZ (diagonal cracks), and the deflection increased suddenly. By increasing the load further, the width of the diagonal cracks increased with a slight gradual decrease in tangent stiffness. Finally, at approximately 94% of P_u (876 kN), a significant reduction of the slope of the load–deflection curve was observed until the failure of the beam. The bottom flexural reinforcement was in the elastic range along the entire response of the specimen P3 (no flexural yielding). As shown in Figure 7, the average strain along the reinforcement measured with DT-A and DT-B reached 1.35×10^{-3} at peak load, which is significantly smaller than the yield strain $\varepsilon_y = 2.63 \times 10^{-3}$.

In addition, Figure 5 shows the crack width measurements at different load levels along the main flexural crack and along the critical diagonal crack. At 87% of P_u, the maximum width of the diagonal crack was observed near the mid-depth of the beam (location 3) and reached a value of ~1.6 mm. On the other hand, the flexural crack was significantly narrower, measuring only ~0.3 mm at the same load level.

While the crack widths were measured at discrete load levels, vertical displacements across the critical diagonal crack w_v were monitored continuously as shown in Figure 8. It can be seen that the displacement near the support (at $0.70a$ from the loading point) and near the load (at $0.25a$ from the loading point) were nearly equal throughout the response of the beam measuring ~1.7 mm at failure. Similarly to the crack widths, w_v was maximum in the mid-depth region, reaching ~2.5 mm at failure.

As the failure of the beam was triggered by crushing in the critical loading zone (CLZ), it is of interest to use the crack measurements to evaluate the deformations in this zone. A suitable approach to evaluate the deformations in the CLZ is the two-parameter kinematic model for deep beams proposed by Mihaylov et al.[16,17] As shown in Figure 9, this approach uses two degrees of freedom (DOFs) to describe the complete displacement field of shear spans with diagonal cracks, including the displacements across the cracks (crack kinematics). The two DOFs are the average strain along the bottom flexural reinforcement, $\varepsilon_{t,avg}$, and the transverse displacement of the critical loading zone, Δ_c. This model has been validated with measured displacement fields and crack data, showing adequate results.[13,14] In fact, it is DOF Δ_c that characterizes the behavior of the CLZ and the shear behavior of deep beams in general. As evident from Figure 9, Δ_c is associated with vertical crack

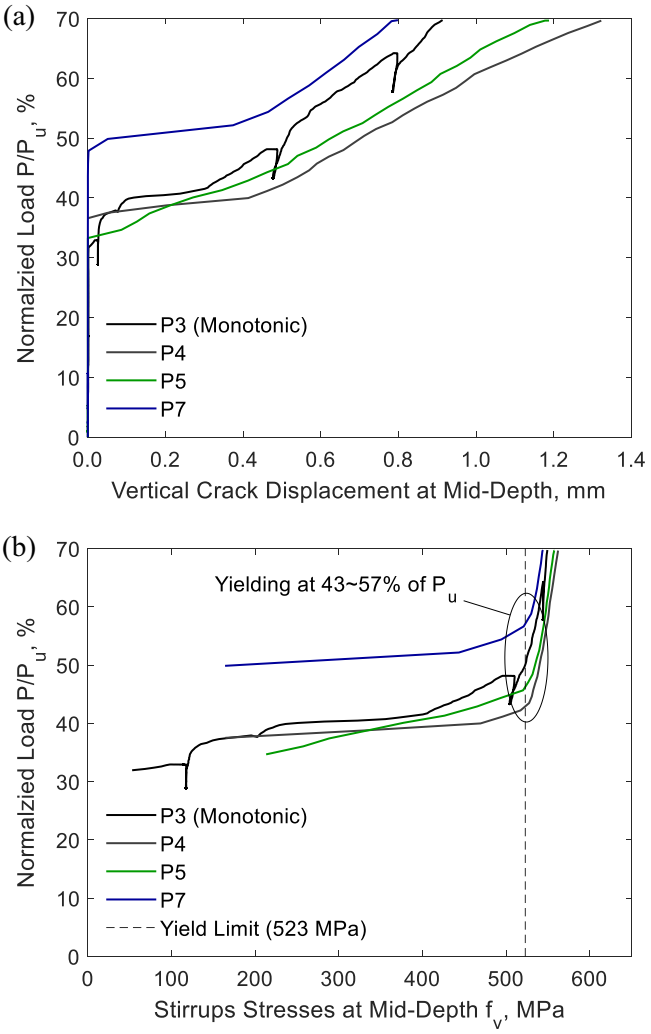

FIGURE 12 Progress of the vertical crack displacement and stirrup stresses at mid-depth in the initial pre-cracking loading stage: (a) Vertical crack displacements and (b) Stirrups stresses. Results of beam P6 is omitted since the critical diagonal shear crack did not cross transducer DT-H.

displacements, which are in turn associated with slip displacements and aggregate interlock stresses across the critical diagonal crack.

Using the kinematic model, the vertical crack displacements are expressed with the two DOFs as follows:

$$w_v = \Delta_c + \varepsilon_{t,avg} l_k \frac{x}{d} \tag{1}$$

where d is the effective depth of the beam, x is the horizontal coordinate measured from the center of the loading plate (positive), and l_k is the portion/length of the flexural reinforcement whose elongation contributes to the opening of the diagonal crack (Figure 9). This linear equation is valid in the middle portion of the crack, where the crack displacements are not affected by the top

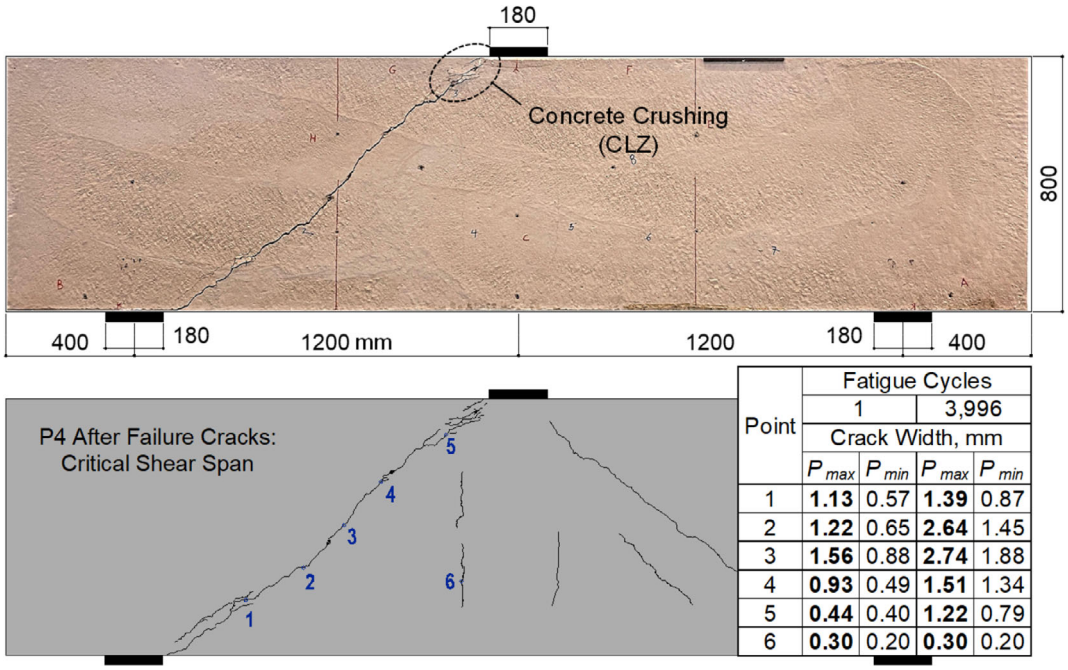

Point	Fatigue Cycles			
	1		3,996	
	Crack Width, mm			
	P_{max}	P_{min}	P_{max}	P_{min}
1	**1.13**	0.57	**1.39**	0.87
2	**1.22**	0.65	**2.64**	1.45
3	**1.56**	0.88	**2.74**	1.88
4	**0.93**	0.49	**1.51**	1.34
5	**0.44**	0.40	**1.22**	0.79
6	**0.30**	0.20	**0.30**	0.20

FIGURE 13 Cracks after failure (top) and crack width measurements at different load levels (bottom)—beam P4.

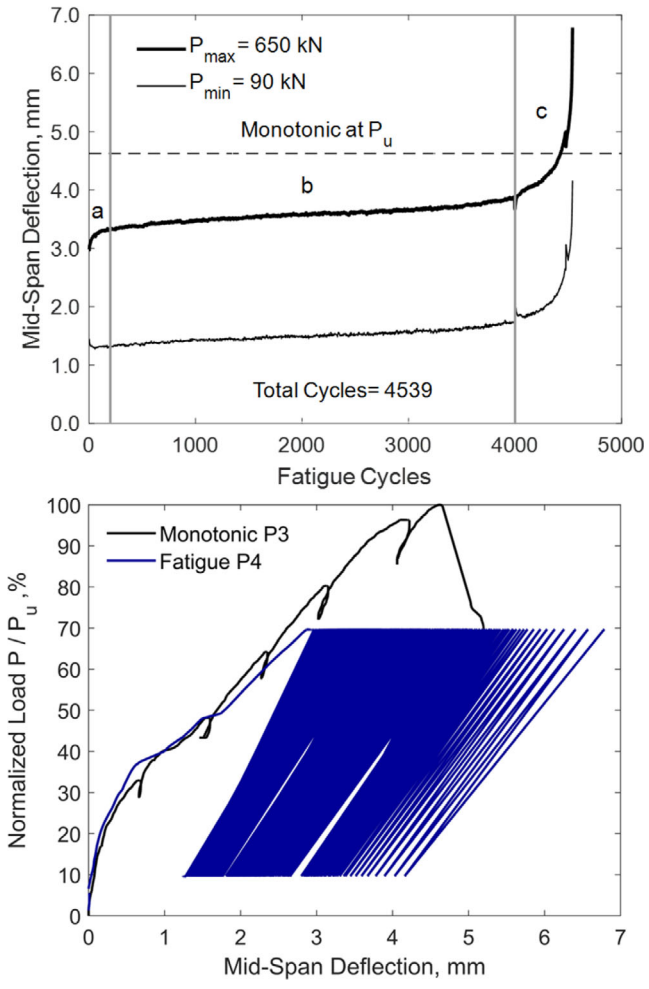

FIGURE 14 Progress of mid-span deflection with the fatigue cycles—beam P4.

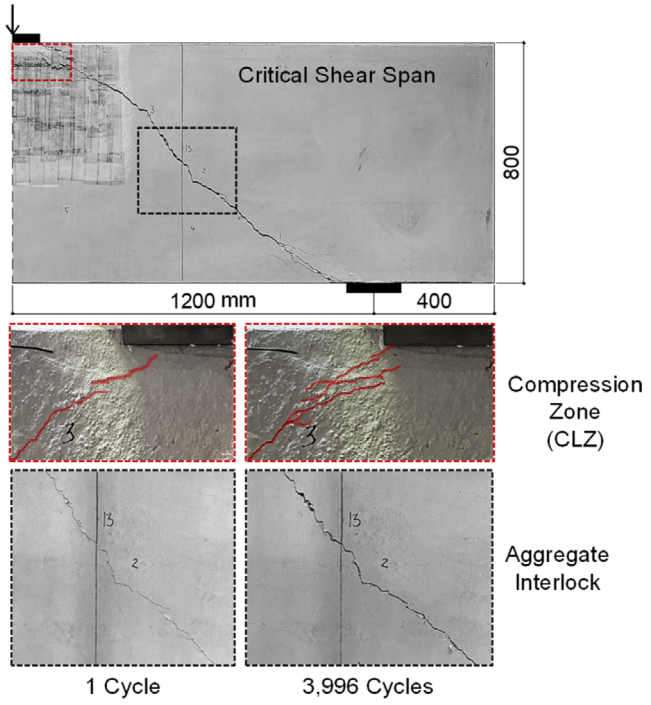

FIGURE 15 Fatigue damage of shear resisting mechanisms—beam P4.

load on the beam and the flexural reinforcement in the bottom of the beam (crack control zone). Vertical displacement transducers DT-F and DT-E were intentionally placed in this portion of the crack, and therefore their measurements can be inserted in the left-hand side of Equation (1). The two measurements provide two

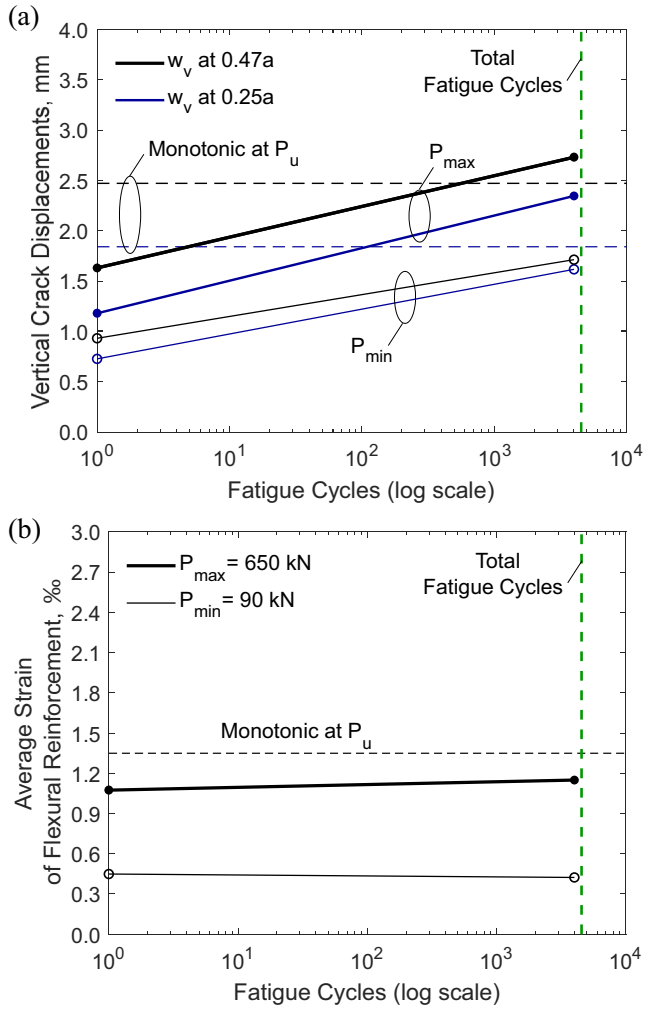

FIGURE 16 Progress of crack displacements and strains with fatigue cycles—beam P4: (a) Vertical crack displacements and (b) Average strain along flexural reinforcement.

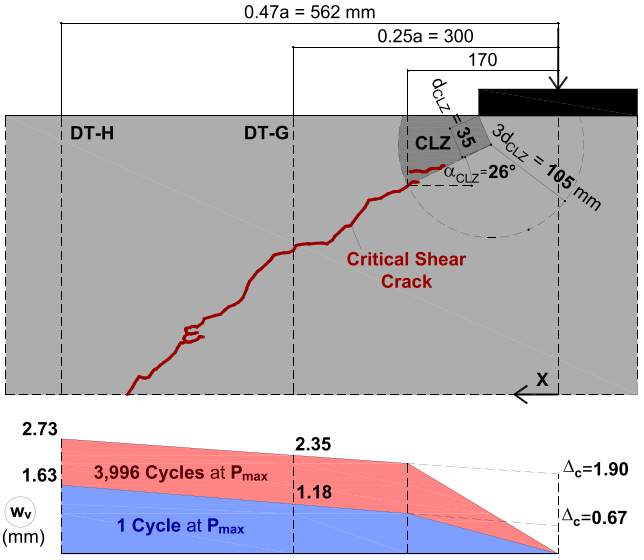

FIGURE 17 Measured geometry of CLZ and estimated DOFΔ_c of kinematic model—beam P4.

simultaneous equations to calculate DOF Δ_c and elongation $\varepsilon_{t,avg} l_k$, where x is either $0.25a$ or $0.47a$.

Figure 10 illustrates the graphical solution of these equations for beam P3 at failure. The two crack displacement readings w_v are connected with a straight line, whose slope is equal to $\varepsilon_{t,avg} l_k / d$. When the line is extended to the center of the load ($x = 0$), it results in a Δ_c value of 1.13 mm at failure. Figure 10 also shows the estimated geometry of the CLZ, which is characterized by two parameters: minimum depth d_{CLZ} and angle α_{CLZ}. Depth d_{CLZ} is measured directly as the shortest distance from the edge of the loading plate to the critical crack (~54 mm), while α_{CLZ} requires to estimate the size of the CLZ along the critical crack. More precisely, angle α_{CLZ} is the inclination of the line connecting the bottom point of d_{CLZ} to the approximate end of the CLZ along the crack. Trandafir et al.[14] have proposed to estimate the length of this line at $3d_{CLZ}$ (~162 mm), which results in an estimated angle α_{CLZ} of 36° for beam P3. The crack diagram shows that displacement transducers DT-E and DT-F are outside the CLZ, and therefore the calculation of Δ_c based on Equation (1) is valid.

With measured d_{CLZ} and α_{CLZ}, the formulation of the critical loading zone derived in Reference 14 allows to estimate the inclined compressive strain along the bottom face of the CLZ—see Equations (2) and (3). For beam P3 at failure, Equation (2) results in an ε_{CLZ} value of $\sim 3 \times 10^{-3}$, which is consistent with the observed crushing of the CLZ.

$$\varepsilon_{CLZ} = \frac{\Delta_c}{3\, l_{b1e}} \tan \alpha_{CLZ} \tag{2}$$

$$l_{b1e} = \frac{d_{CLZ}}{\sin \alpha_{CLZ}} \tag{3}$$

3.2 | Fatigue tests

As previously mentioned, the beams used for fatigue testing were initially loaded monotonically up to 70% of P_u (650 kN) in order to create diagonal shear cracks. Afterwards, the beams were subjected to fatigue cycles up to failure. Figure 11 illustrates the global response of the beams during the initial monotonic pre-cracking phase, together with the complete response of the reference specimen P3. It can be seen that the initial stiffness of the four beams was nearly identical, which is also consistent with the small variation of the modulus of elasticity of the concrete (Table 1). However, there is a more visible variation in the stiffness of the beams after the formation

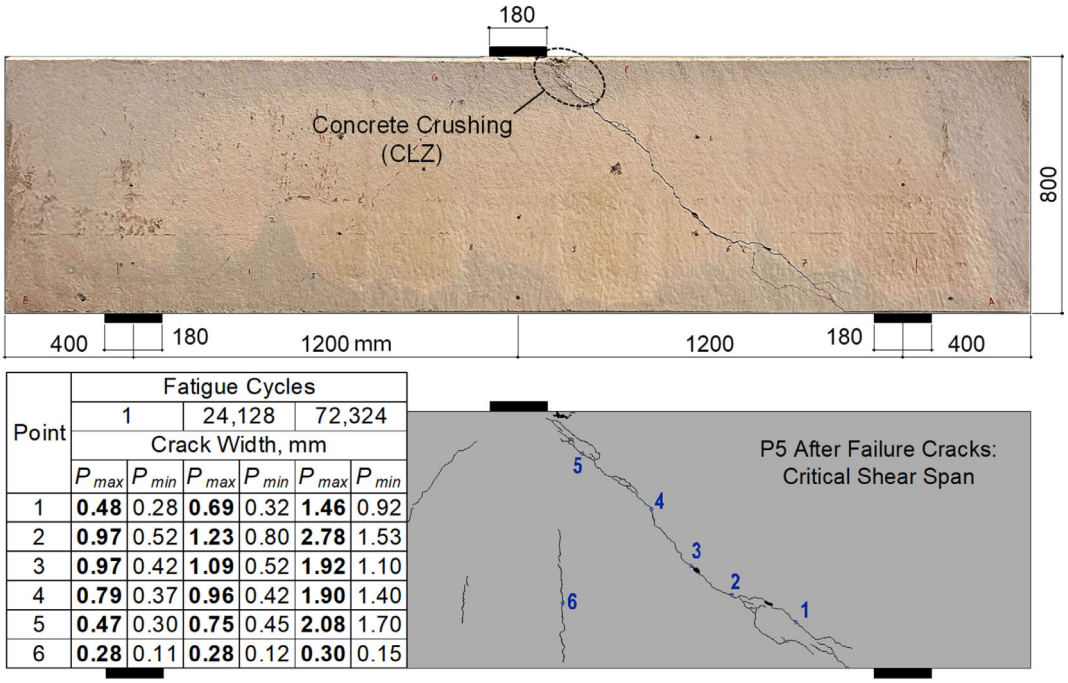

Point	Fatigue Cycles					
	1		24,128		72,324	
	Crack Width, mm					
	P_{max}	P_{min}	P_{max}	P_{min}	P_{max}	P_{min}
1	**0.48**	0.28	**0.69**	0.32	**1.46**	0.92
2	**0.97**	0.52	**1.23**	0.80	**2.78**	1.53
3	**0.97**	0.42	**1.09**	0.52	**1.92**	1.10
4	**0.79**	0.37	**0.96**	0.42	**1.90**	1.40
5	**0.47**	0.30	**0.75**	0.45	**2.08**	1.70
6	**0.28**	0.11	**0.28**	0.12	**0.30**	0.15

FIGURE 18 Cracks after failure (top) and crack width measurements at different load levels (bottom)—beam P5.

of diagonal shear cracks, with beams P4 and P5 exhibiting softer response than the other three beams. This difference is attributed mainly to random variations in the path of the critical cracks.[14]

The softer response of beams P4 and P5 is also observed in the measured vertical crack displacements, as shown in Figure 12a. In the middle zone of the diagonal cracks ($x = 0.47a$) at 70% of P_u, w_v of beams P4 and P5 was approximately 1.5 larger than the corresponding measurements in beams P1 and P7. These crack displacements are used together with a bond model proposed by Sigrist[18] to evaluate the stress in the stirrups f_v in the cracks. In this model, the bond stress along the bar is a function of the tensile strength of the concrete f_{ct}, which estimated at $0.26f_c'^{2/3}$ (MPa). The bars are assumed anchored in two uncracked concrete blocks, one on each side of the critical crack. As evident from the results in Figure 12b, the stirrups in beams started yielding and entered the strain-hardening regime ($f_v > f_{yv} = 523$ MPa) at 43%–57% of P_u in the initial monotonic pre-cracking phase.

3.2.1 | Fatigue test of beam P4

Beam P4 was subjected to fatigue cycles with $P_{max} = 650$ kN (70% of P_u) and $P_{min} = 90$ kN (9.7% of P_u), after the specimen was pre-cracked with diagonal shear cracks at a load of 70% of P_u. The beam failed at 4,539 cycles with crushing of the critical loading zone (CLZ) and opening of a critical diagonal crack as shown in Figure 13.

As evident from Figure 14 (top), the progress of the mid-span deflection with fatigue cycles at P_{max} and P_{min} was characterized by three phases: (a) an initial fast increase up to ~200 cycles due to cyclic creep; (b) a slow linear increase from ~200 cycles to ~4,000 cycles; and (c) a rapid increase after ~4,000 cycles up to failure. This trend is similar to the fatigue behavior of concrete in uniaxial compression as reported elsewhere.[19] Crack widths were measured in the beginning of the test (1st cycle) and near the end of the second phase (at ~4,000 cycles) as shown in the crack diagram in Figure 13. It is evident that the flexural cracks remained unchanged, while the width of the critical diagonal crack increased substantially.

Figure 14 (bottom) shows the fatigue response of beam P4 in terms of load versus mid-span deflection, in comparison to the monotonic response of beam P3. The unloading and reloading stiffness decreased with increasing number of cycles, while the mid-span deflection increased and surpassed the deflection of P3 at peak load. Beam P4 failed at a deflection of 6.8 mm, which is 48% larger than the failure deflection measured in the monotonic test.

The fatigue damage observed in beam P4 is illustrated in Figure 15 with photographs taken in the beginning of the test (1st cycle) and near the end of the second phase (at ~4,000 cycles). The damage was associated mainly with two shear-resisting mechanisms: the inclined

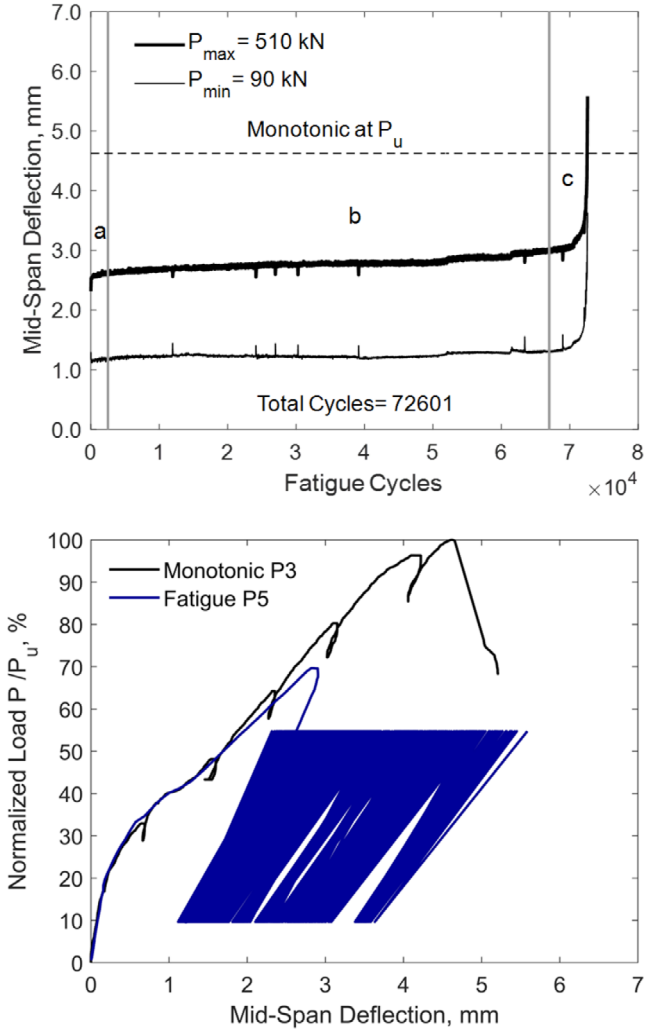

FIGURE 19 Progress of mid-span deflection with the fatigue cycles—beam P5.

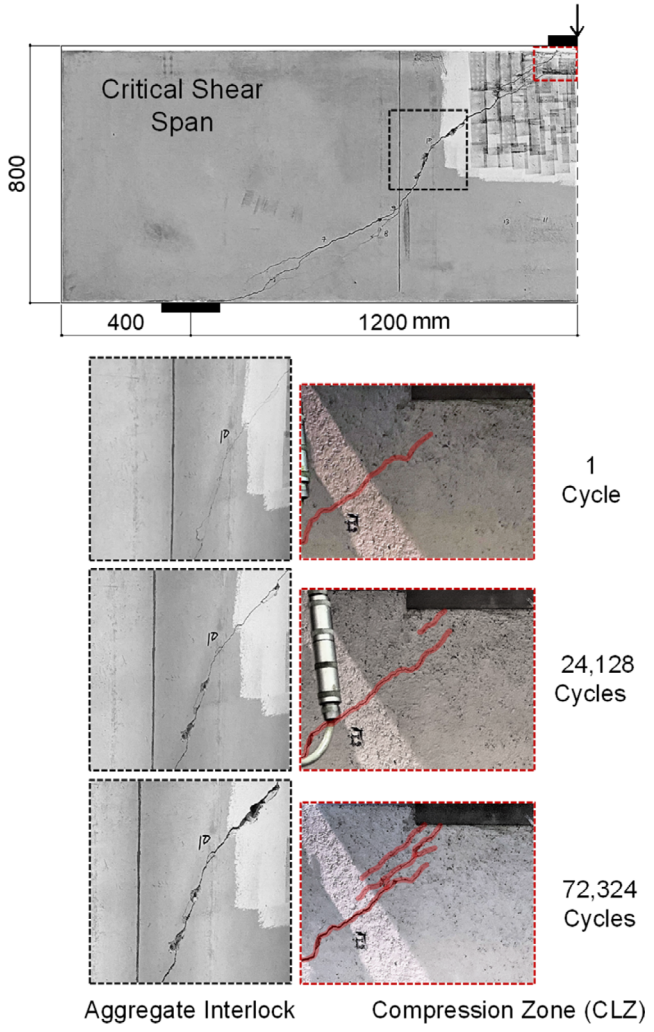

FIGURE 20 Fatigue damage of shear resisting mechanisms—beam P5.

compression in the critical loading zone and the aggregate interlock across the critical crack. It can be seen that the load cycles caused inclined macro cracks in the CLZ, which eventually led to fatigue crushing of the concrete in this zone. Moreover, during the fatigue cycles, the crack edges were eroded, and the crack interface was gradually smoothened, in particular along the steepest segments of the critical crack. The steepest segments develop the largest slip displacements and corresponding aggregate interlock stresses, and therefore their deterioration is linked to significant reduction in shear resistance.[14]

During the fatigue cycles, the vertical displacements across the critical diagonal crack increased as shown in Figure 16a. At ~4,000 cycles, w_v at P_{max} at $x = 0.47a$ and $0.25a$ increased respectively by ~67% and ~99% compared to the displacements in the 1st cycle. At the same time, the average strains in the flexural reinforcement remained nearly unchanged (7% increase)—see Figure 16b. These results are consistent with the evolution of the widths of the shear and flexural cracks reported in Figure 13. They show that the fatigue behavior of the beam was governed by shear strength deterioration, while the flexural resistance was not affected significantly.

This can also be illustrated with the help of the two-parameter kinematic model in Figure 9. According to the model, the flexural deformation pattern associated with DOF $\varepsilon_{t,avg}$ remained nearly unchanged, while the shear pattern associated with DOF Δ_c exhibited increasing deformations under consecutive fatigue cycles up to failure. Figure 17 shows the variation of the vertical displacements along the critical crack, including DOF Δ_c defined at the center of the loading plate. Between cycle 1 and ~4000, Δ_c increased from 0.67 mm to 1.90 mm, and the corresponding estimated strain in the CLZ increased from 1.4×10^{-3} to 3.9×10^{-3} (Equations 1–3). Therefore, the CLZ of beam P4 failed with a maximum

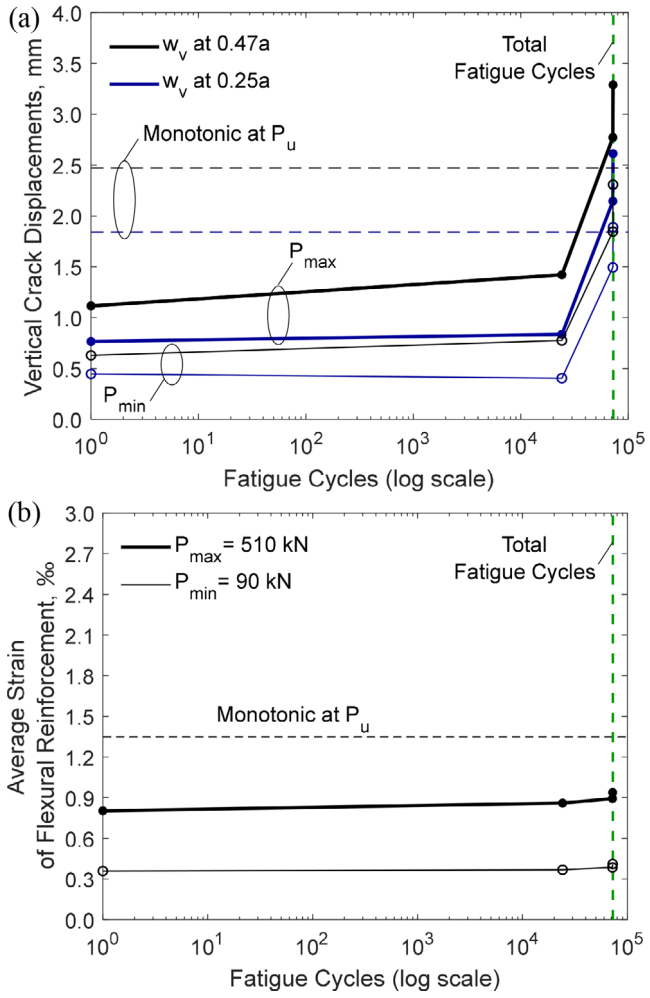

FIGURE 21 Progress of crack displacements and strains with fatigue cycles—beam P5: (a) Vertical crack displacements and (b) Average strain along flexural reinforcement.

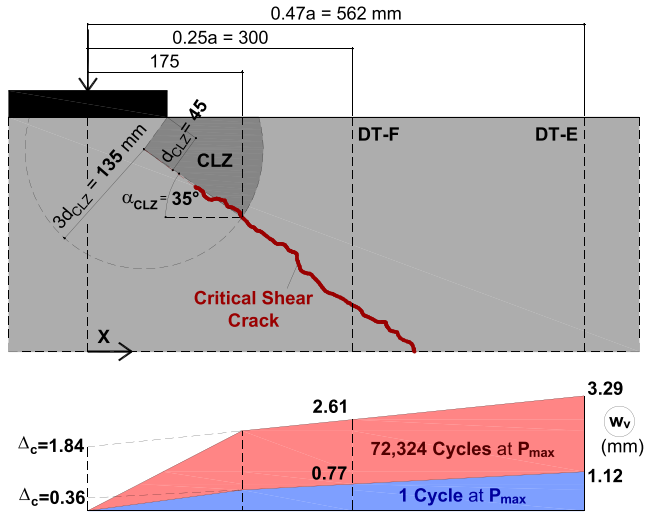

FIGURE 22 Measured geometry of CLZ and estimated DOFΔ_c of kinematic model—beam P5.

compressive strain which is 30% larger than that in the monotonic test. This is due to the accumulated irreversible compressive strains and reduction of stiffness of the CLZ caused by the formation of microcracks during the fatigue loading.[19]

3.2.2 | Fatigue test of beam P5

Beam P5 was subjected to fatigue cycles with $P_{\max} = 510$ kN (54.7% of P_u) and $P_{\min} = 90$ kN (9.7% P_u), after the specimen was pre-cracked with diagonal shear cracks at a load of 70% of P_u. Similarly to beam P4, the failure occurred with crushing of the CLZ and opening of a critical diagonal crack as shown in Figure 18. However, the reduction of $P_{\max}$ from 70% to 55% of P_u resulted in a substantial difference in the number of load cycles to failure: 4,539 for P4 versus 72,601 for P5.

The increase of mid-span defection with the number of load cycles, as well as the load–deflection response of beam P5 in comparison to the monotonic test P3, are shown in Figure 19. As in test P4, the progress of the mid-span deflection at $P_{\max}$ and $P_{\min}$ is characterized by three phases: (a) an initial fast increase up to ~2,500 cycles due to cyclic creep; (b) a slow linear increase from ~2,500 cycles to ~67,000 cycles; and (c) a rapid increase after ~67,000 cycles up to failure. The crack width measurements in Figure 18 were performed in the 1st cycle, at 24,128 cycles, and near the end of the third phase at 72,324 cycles. The damage associated with the concrete shear-resisting mechanisms at these three stages is illustrated with photographs in Figure 20. As before, inclined macro cracks accumulated in the CLZ, and the surfaces of the critical crack were severely eroded due to cyclic aggregate interlock.

Clear evidence that the fatigue behavior of beam P5 was governed by shear, as presented in Figure 21. Just prior to failure, the vertical displacements in the diagonal cracks at $x = 0.47a$ and $0.25a$ at $P_{\max}$ increased respectively by ~2.9 times and ~3.4 times compared to the values in the 1st load cycle. At the same time, the average strain in the flexural reinforcement exhibited only a slight increase, and no flexural damage was visible during the fatigue testing. Just before failure, the average strain at $P_{\max}$ had increased by only ~17% compared to the value in the 1st load cycle. In other words, the flexural fatigue damage was not dominant, and the failure of the beam was caused by the fatigue damage of the shear-resisting mechanisms.

In terms of measured geometry of the critical loading zone, beam P5 represented an intermediate case between P3 and P4—see Figure 22. The depth d_{CLZ} was ~45 mm and the angle α_{CLZ} was ~35°. The shear DOF associated

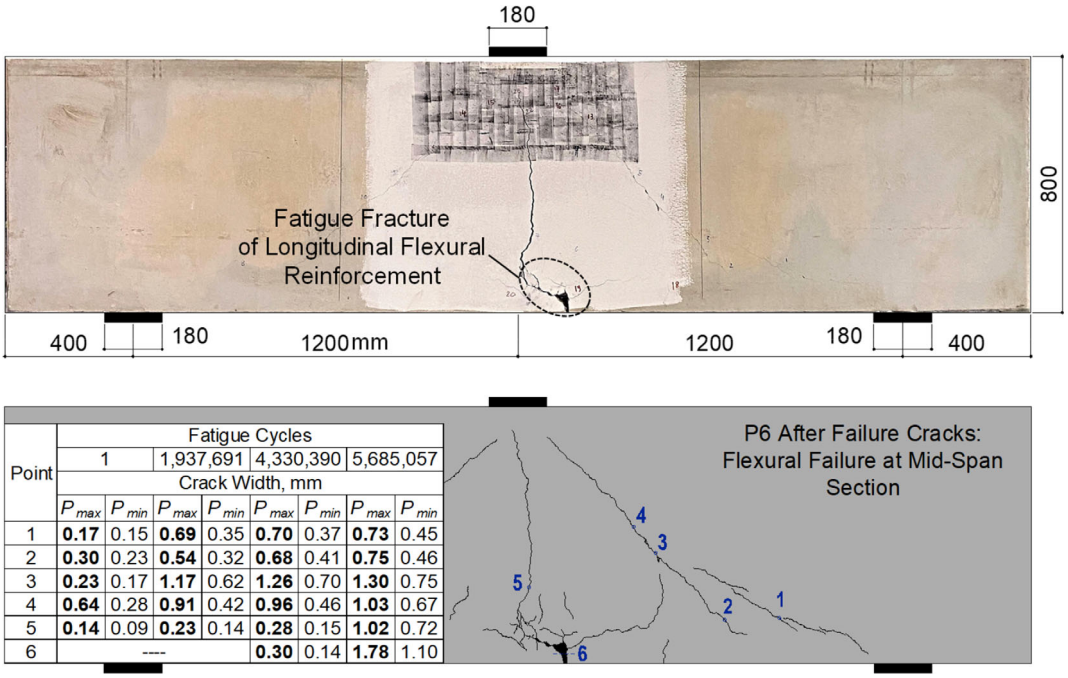

Point	Fatigue Cycles							
	1		1,937,691		4,330,390		5,685,057	
	Crack Width, mm							
	P_{max}	P_{min}	P_{max}	P_{min}	P_{max}	P_{min}	P_{max}	P_{min}
1	**0.17**	0.15	**0.69**	0.35	**0.70**	0.37	**0.73**	0.45
2	**0.30**	0.23	**0.54**	0.32	**0.68**	0.41	**0.75**	0.46
3	**0.23**	0.17	**1.17**	0.62	**1.26**	0.70	**1.30**	0.75
4	**0.64**	0.28	**0.91**	0.42	**0.96**	0.46	**1.03**	0.67
5	**0.14**	0.09	**0.23**	0.14	**0.28**	0.15	**1.02**	0.72
6	---				**0.30**	0.14	**1.78**	1.10

FIGURE 23 Cracks after failure (top) and crack width measurements at different load levels (bottom)—beam P6.

with the CLZ increased from 0.36 mm in the 1st cycle to 1.84 mm at cycle 72,324 near failure (~5-times increase). The corresponding compressive strain in the CLZ is estimated to have increased from 1.1×10^{-3} to 5.5×10^{-3}, reaching larger values than in beam P4.

3.2.3 | Fatigue testing of beam P6

Beam P6 was subjected to fatigue cycles with $P_{max} = 420$ kN (45.1% of P_u) and $P_{min} = 90$ kN (9.7% P_u), after the specimen was pre-cracked with diagonal shear cracks at a load of 70% of P_u. At ~2.4 million cycles, a short fatigue flexural crack propagated suddenly in the bottom of the beam near the main flexural crack at mid-span. When the short crack merged with the main crack and extended to ~90% of the total depth of the beam at 5,685,066 cycles, the fatigue loading was stopped. At this point, it was evident that the beam would fail in flexure. In order to have a clear failure, the beam was then unloaded and reloaded monotonically in displacement control (rate ~0.01 mm/s) up to failure. The failure occurred due to fatigue fracture and yielding of the flexure reinforcement at a total load of 671 kN (72% of P_u) as shown in Figure 23.

Compared to beams P4 and P5, the progress of the mid-span deflection with the fatigue cycles at P_{max} and P_{min} also had three apparent phases, but differed in the final phase (Figure 24 top): (a) an initial fast increase up to ~40,000 cycles due to cyclic creep; (b) a linear increase from ~40,000 cycles to ~2 million cycles; and (c) a stepwise increase after ~2 million cycles up to failure. Accordingly, Figure 23 shows detailed crack width measurements after the first load cycle, at ~2 million cycles, at ~4.3 million cycles, and at the end of the final third phase. Up to ~2.4 million cycles, the increase of the width of the shear crack was larger than that of the flexural cracks. After this stage, the flexural cracks widened significantly and dominated the response up to failure.

A more detailed illustration of this transition between shear and flexural modes is demonstrated in Figure 25a, which compares the evolution of crack widths at three different locations. A comparison is made between the diagonal shear crack (point 4 in Figure 23), the main flexural crack (point 5 in Figures 23 and 25c), and the short flexural crack (point 6 in Figure 23 and 25c). The propagation of the two flexural cracks with increasing number of cycles is shown in Figure 25c. Before the formation of the short flexural crack at ~2.4 million cycles, the diagonal shear crack widened up to ~1.2 mm, while the opening of the main flexural crack had a slight increase due to the deterioration of the bond and tension stiffening of the flexural reinforcement. After the formation of the short flexural crack, the opening of the shear crack stabilized, and the behavior was dominated by the opening and propagation of the two flexural cracks. At the end of the fatigue cycles, the short flexural crack had merged with the main flexural crack and had reached a width of ~1.8 mm.

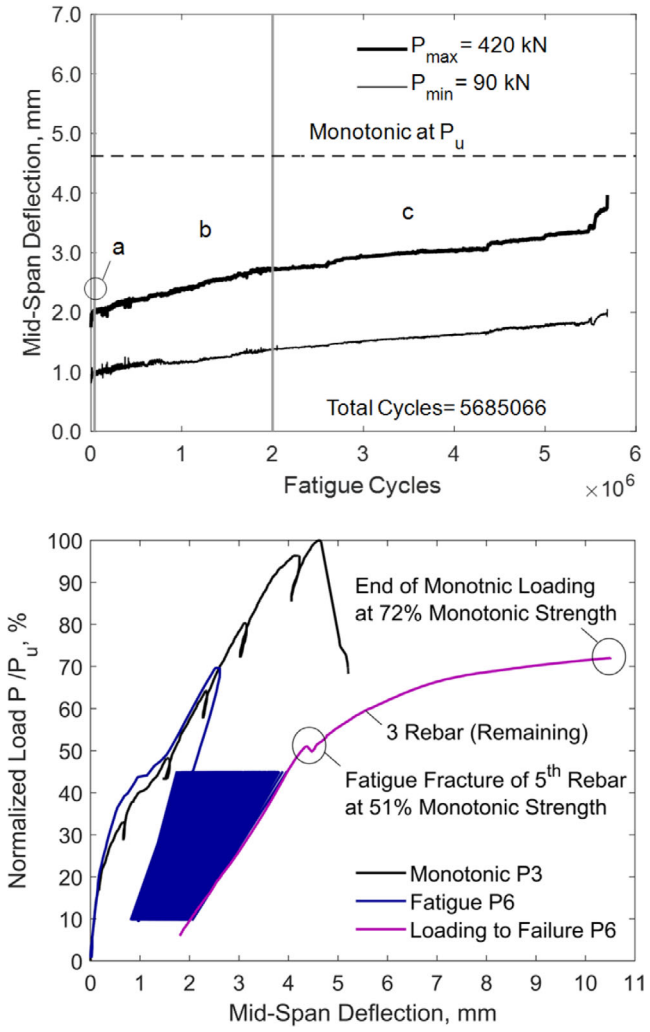

FIGURE 24 Progress of mid-span deflection with the fatigue cycles—beam P6.

In the flexure-dominated regime after ~2.4 million cycles, the stepwise increase of mid-span deflection is explained with the help of Figure 25b. The plot matches the evolution of the deflection at P_{max} with the evolution of the width of the short flexural crack (two-axes plot). It can be seen that the sudden increases (steps) in the mid-span deflection occurred simultaneously with four rapid increases of the crack width. These steps are devoted to fatigue fractures of four out of the eight bottom longitudinal bars, which was confirmed after the test by removing the concrete cover.

Figure 24 (bottom) shows the complete load–deflection fatigue response of beam P6 in comparison to the monotonic response of P3. At the end of the fatigue cycles, the deflection reached ~4.0 mm, which is smaller than the deflection of P3 at failure (~4.6 mm). The plot also shows the final monotonic response of beam P6 when the specimen was loaded to failure in displacement control. At a load of 475 kN (51% of P_u), a fifth longitudinal bar fractured, and the resistance dropped, before it quickly increased again with increasing displacement. This increase was due to the strain-hardening of the remaining three longitudinal bars in the critical flexural crack. The test was stopped at 671 kN (72% of P_u) when the load–deflection curve flattened.

The five fractured bars are shown in the photographs in Figure 26a taken after the test. The fractures occurred due to defects and stress concentrations at the locations where the bars were tack-welded to the stirrups and to the steel connectors used for placing the second layer of the flexural reinforcement (Figure 1). These premature fractures are consistent with past experimental studies.[20] It has been reported that tack-welding of stirrups to longitudinal bars reduces the endurance fatigue limit of the bars by 28%–50%, where the endurance limit is the stress range below which the bar can endure an infinite fatigue life.

Since the stress range f_r is the major factor for fatigue behavior of steel bars,[2] it is of interest to evaluate the stresses in the longitudinal reinforcement of beam P6. The stress in the eight bars just before the first fracture can be estimated using the free body diagram in Figure 26b. Based on the crack diagram at this stage, the lever arm of the internal longitudinal forces in the mid-span section is estimated at $z \approx 613$ mm. With this lever arm and the applied loads P_{min} and P_{max}, the total tension force in the bars is evaluated to have varied between $T_{min} = 83$ kN and $T_{max} = 389$ kN, and the corresponding stress between $f_{s,min} = 33$ MPa and $f_{s,max} = 155$ MPa. Therefore, the stress range that caused the first bar fracture was $f_r = f_{s,max} - f_{s,min} = 122$ MPa. Based on the model by Helgason and Hanson,[21] the lowest average endurance limit for straight bars is ~165 MPa. This limit is 35% larger than the stress range in beam P6, but it does not account for the effect of tack welding. Due to the tack welding in beam P6, the limit was likely reduced by 28%–50% (~83–119 MPa), and thus the bar fractured after experiencing ~2.7 million cycles.

When the same analysis is performed at the end of the final monotonic loading ($P = 671$ kN and $z \approx 696$ mm), the stress in the three remaining bars is estimated at 635 MPa, which is almost equal to the ultimate tensile strength of the steel ($f_u = 616$ MPa). This result demonstrates that the fatigue cycles did not cause a reduction of the monotonic tensile strength of these three bars.

3.2.4 | Fatigue testing of beam P7

Beam P7 was subjected to fatigue cycles with $P_{max} = 510$ kN (54.7% of P_u) and $P_{min} = 210$ kN (22.5% of P_u), after the specimen was pre-cracked with diagonal

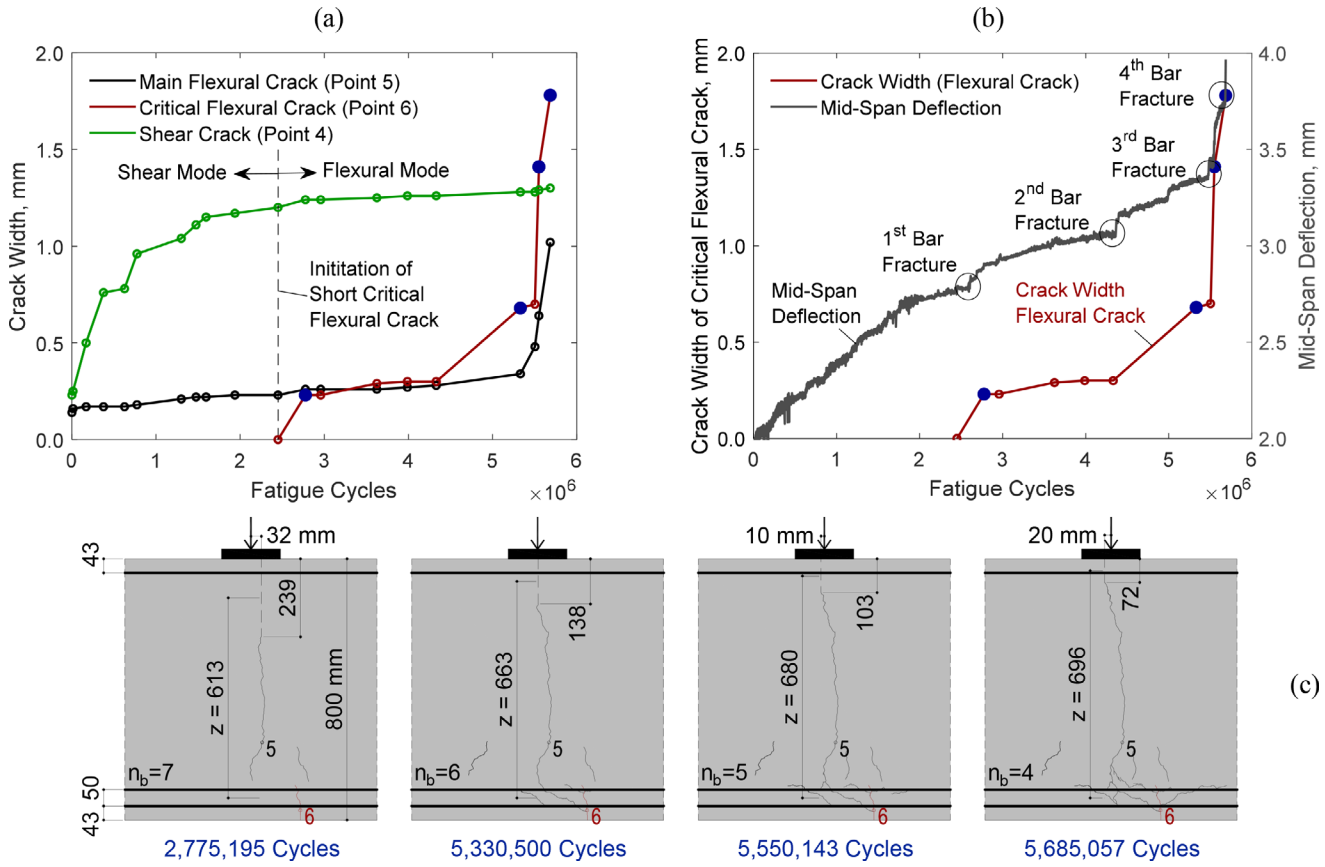

FIGURE 25 Progress of flexural cracks with the fatigue cycles—beam P6: (a) Comparison of flexural and shear cracks, (b) Fatigue fracture of flexural bars, and (c) Flexural cracks propagation (n_b is the number of non-fractured bottom bars).

shear cracks at a load of 70% of P_u. After approximately 1 million cycles, a macro-crack was observed in the CLZ of the critical shear span. As the fatigue testing continued, more macro-cracks and concrete crushing of some parts occurred in the CLZ. The fatigue testing was stopped after 4,595,798 cycles and the beam was loaded monotonically in displacement control (rate ~0.01 mm/s) up to failure. The failure occurred with crushing of the CLZ and opening of a critical diagonal crack at a total load of 758 kN (81% of P_u) as shown in Figure 27.

Although beam P7 experienced a failure mode similar to that of beams P4 and P5, the progress of the mid-span deflection with the number of cycles at P_{max} and P_{min} was different and can be characterized by four phases—see Figure 28 (top): (a) an initial fast increase up to ~160,000 cycles due to cyclic creep; (b) a linear increase from ~160,000 cycles to ~800,000 cycles; (c) a slower linear increase from ~800,000 cycles to ~4.6 million cycles; and (d) a rapid increase after ~4.6 million cycles near failure. Accordingly, the crack width measurements in Figure 27 were performed at the 1st cycle, ~160,000 and ~800,000 cycles, and near the end of the last phase. While the width of both shear and flexural cracks increased with the fatigue cycles, the increase of the shear crack was significantly larger from 0.48 mm after the 1st cycle to 2.44 mm near failure. Similarly to beams P4 and P5, the surfaces of the shear crack were eroded due to cyclic aggregate interlock, and accumulation of damage was observed in the CLZ.

Figure 28 (bottom) shows the cyclic load–deflection response of beam P7 compared to the monotonic response of beam P3. The response of the two beams during the pre-cracking stage 70% of P_u was similar. After the application of the fatigue cycles at constant load levels (~4.6 million cycles), the mid-span deflection of beam P7 increased up to ~4.5 mm, which is approximately equal to the deflection at failure of P3 (~4.6 mm). Then by loading the beam monotonically up to failure, P7 reached its peak load at 81% of the monotonic strength and a deflection of 5.6 mm, which is 22% higher than in the monotonic test.

The vertical crack displacements increased during the fatigue cycles as shown in Figure 29a, while the increase of flexural strain is illustrated in Figure 29b. Near the end of the fatigue cycles, w_v at $x = 0.47a$ and $0.25a$ under P_{max} increased ~3.4 times and ~4.5 times, respectively, compared to their displacements in the 1st cycle. The average strain in the flexural longitudinal reinforcement

at P_{max} increased by 33%. Since no flexural damage was observed during the fatigue testing, this increase may be explained with additional crack opening of the diagonal cracks at the level of the flexural reinforcement and loss of tensing stiffening of the reinforcement due to bond fatigue damage. Generally, the bond degradation is a slow process that requires millions of load cycles to have a significant impact.[22] In the end, the flexural fatigue damage was not dominant for the ultimate response of the beam, and the failure was caused by the fatigue of the shear-resisting mechanisms.

This is consistent with the shear degree of freedom of the kinematic model Δ_c, which is estimated from the measured vertical crack displacements as shown in Figure 30. At the end of the fatigue cycles at P_{max}, Δ_c reached ~1.26 mm, which is ~23-times larger than the value in the 1st cycle in demonstration of the fatigue compression damage in the CLZ. Finally, the corresponding maximum compressive strain in the CLZ estimated from Equations (2) and (3) reached $\sim 6 \times 10^{-3}$.

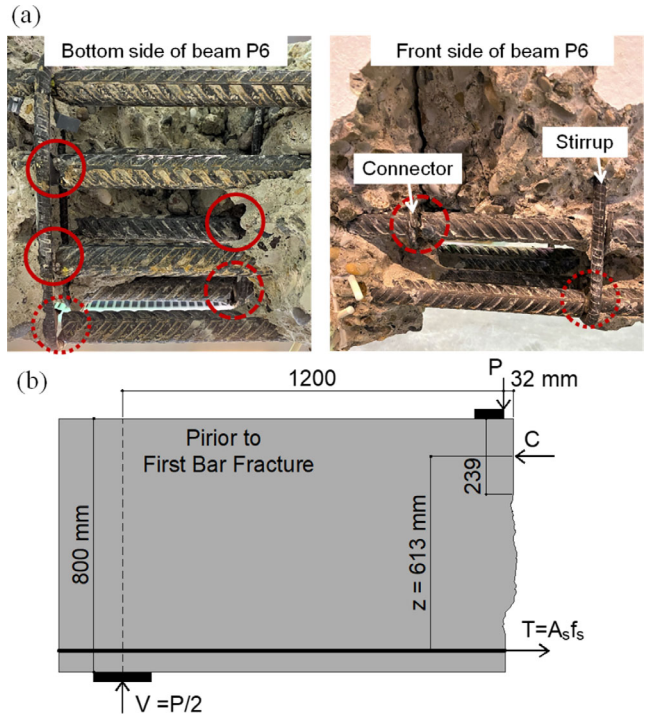

FIGURE 26 Fracture and estimation of stresses in longitudinal flexural reinforcement—beam P6: (a) Fatigue fracture of reinforcement and (b) Free body diagram prior to first bar fracture.

4 | SUMMARY OF TEST RESULTS

Figure 31 shows a comparison of the global response of the beams tested in fatigue in terms of mid-span deflection versus the number of load cycles. Beams P4, P5, and P7 failed in shear by crushing of the CLZ, however, beam P7 exhibited a more gradual failure due to more bond fatigue damage along the flexural reinforcement. On the other hand, beam P6 failed in flexure by fatigue fracture of the bottom longitudinal reinforcement.

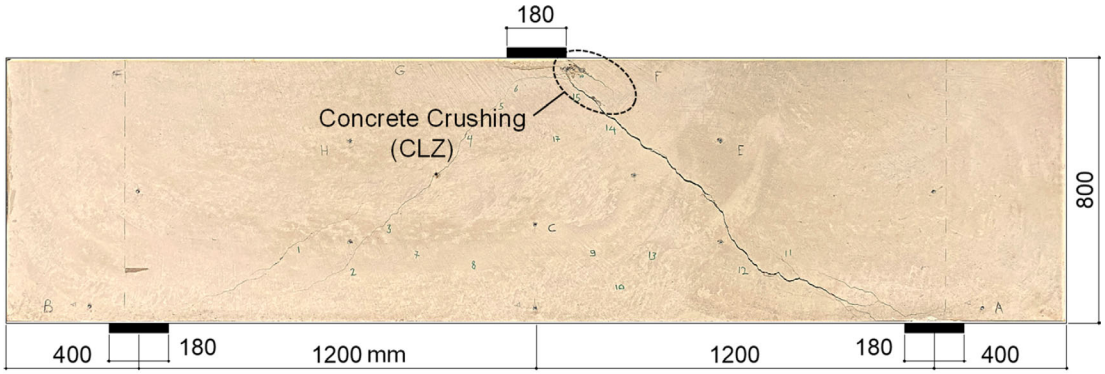

Point	Fatigue Cycles							
	1		157,200		798,362		4,563,536	
	Crack Width, mm							
	P_{max}	P_{min}	P_{max}	P_{min}	P_{max}	P_{min}	P_{max}	P_{min}
1	**0.48**	0.36	**0.53**	0.37	**1.39**	0.84	**2.44**	1.77
2	**0.59**	0.41	**0.68**	0.42	**1.37**	0.96	**2.12**	1.64
3	**0.34**	0.21	**0.42**	0.27	**0.99**	0.68	**1.88**	1.43
4	**0.42**	0.28	**0.58**	0.35	**0.88**	0.68	**1.85**	1.39
5	**0.21**	0.12	**0.24**	0.19	**0.44**	0.39	**1.13**	0.99
6	**0.08**	0.06	**0.12**	0.09	**0.13**	0.10	**0.16**	0.12

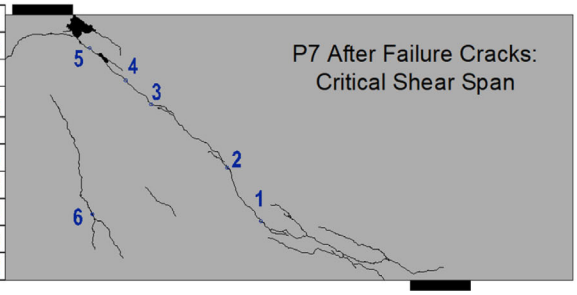

FIGURE 27 Cracks after failure (top) and crack width measurements at different load levels (bottom)—beam P7.

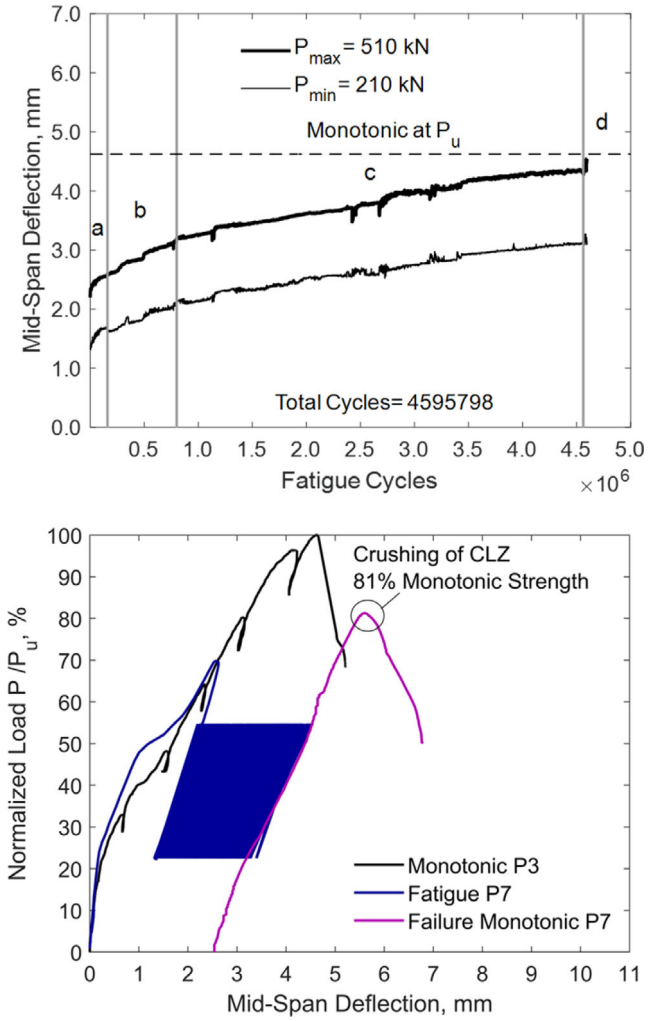

FIGURE 28 Progress of mid-span deflection with the fatigue cycles—beam P7.

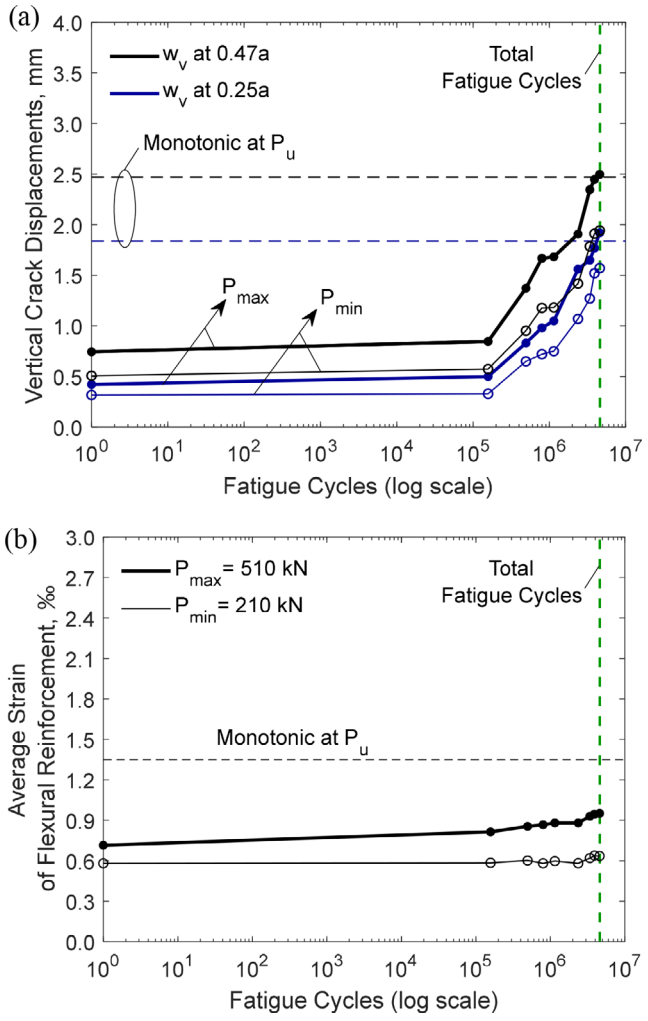

FIGURE 29 Progress of crack displacements and strains with fatigue cycles—beam P7: (a) Vertical crack displacements and (b) Average strain in flexural reinforcement.

The first variable in the test series was the maximum fatigue load P_{max}, which is investigated using the results from beams P3 to P6. Figure 32a shows the load level P_{max}/P_u versus the number of failure cycles (P–N diagram) obtained from these four beams. The black solid line is the trend line defined by the experimental results of beams P3, P4 and P5 (black dots), since these specimens had the same failure mode. At load levels P_{max}/P_u above ~50%, it is evident that the beams tend to fail in shear by crushing of the CLZ. On the other hand, below that range, the expected failure is flexural with fracture of the longitudinal reinforcement in the presence of stress concentrators (e.g., tack welds). As it can be expected, when the maximum fatigue load is reduced, the fatigue life of the CLZ and the beam is prolonged. This can lead to the initiation of fatigue flexural crack at the locations of welds and/or imperfections along the flexural reinforcement. Eventually, fatigue flexural failure can occur before the crushing of the CLZ. Based on beams P4 and

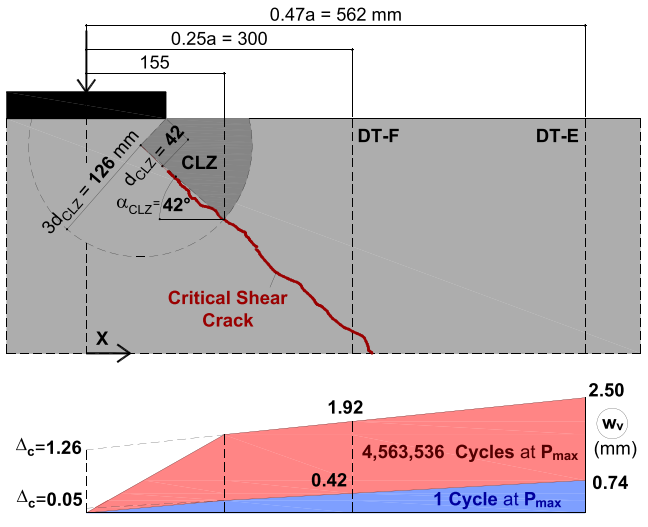

FIGURE 30 Measured geometry of CLZ and estimated DOFΔ_c of kinematic model—beam P7.

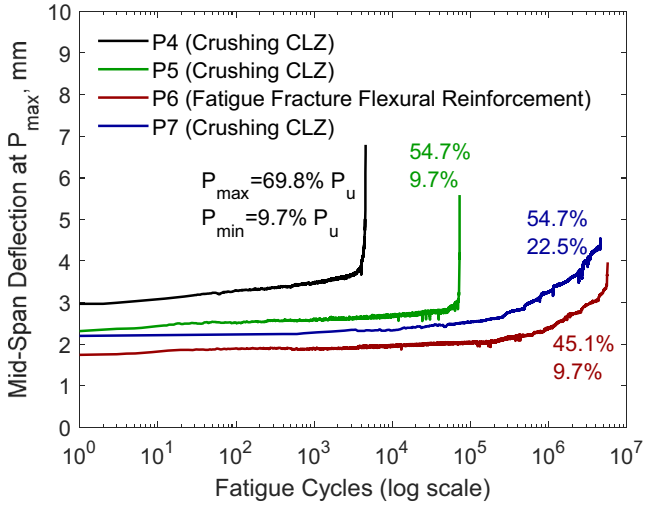

FIGURE 31 Comparison of the fatigue response of tested deep beams.

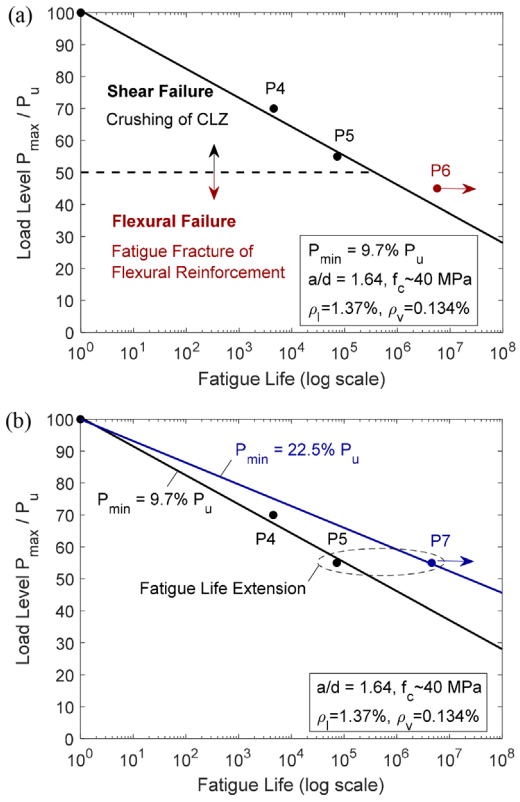

FIGURE 32 Load cycles versus fatigue life (*P–N* diagrams) of tested deep beams: (a) *P–N* diagram for test variable P_{max} and (b) *P–N* diagram for test variable P_{min}.

P5 in the shear-failure range of the *P–N* diagram, when the maximum load P_{max} is reduced by ~22%, the fatigue life is extended 16 times.

The second variable in the test series was the minimum fatigue load P_{min}, which is investigated using the results of beams P5 and P7. Figure 32b shows the *P–N* diagram that includes these beams. The black solid line is the trend line defined by the test results from beams P3, P4 and P5 (black dots) with a P_{min} of 9.7% of P_u. The blue solid line is the trend line based on the results from beams P3 and P7 (blue dots) with a P_{min} of 22.5% of P_u. From these two lines, it is evident that P_{min} has a substantial impact on the fatigue life of deep beams, and this impact is more significant as P_{max} decreases due to the reduction of stress-range of the shear resisting components. Based on the experimental results of beams P5 and P7, when P_{min} increased ~2.3 times, the fatigue life of beam P7 is extended by more than 63 times.

TABLE 4 Predicted shear strength of beam P3 according to 2PKT.[16]

Predicted shear strength components (kN)				
V_{CLZ}	V_{ci}	V_s	V_d	$V_{pred.}$
212	179	129	6	526
$V/V_{pred.}$ (%)				
40	34	25	1	100

5 | DISCUSSION ON SHEAR RESISTING MECHANISMS UNDER FATIGUE LOADING

The shear resisting mechanisms of the monotonic reference beam (P3) can be predicted by using the 2PKT approach.[16] According to the 2PKT, the shear is carried by four mechanisms: diagonal compression in the CLZ, V_{CLZ}, shear transfer by aggregate interlock along the diagonal shear crack, V_{ci}, tension in the transverse reinforcement (stirrups), V_s, and shear resisted by the dowel action of the longitudinal flexural reinforcement, V_d. Table 4 summarizes the predicted shear resisting components and shear strength of specimen P3. The 2PKT captures reasonably well the shear strength with an experimental-to-predicted ratio $V_{exp.}/V_{pred.} = 466/526 = 0.89$. According to the 2PKT results, most of the shear is carried by the CLZ and the transverse reinforcement: 40% and 34%, respectively. The aggregate interlock contribution is 25%, while the dowel action of the flexural reinforcement is negligible.

During the fatigue cycles in the case of the beams failing in shear, the shear resisting mechanisms, and mainly the CLZ and the aggregate interlock, deteriorate with the number of cycles as demonstrated from the experimental observations. The rate of deterioration of these components depends on the stress levels that they experience

under the applied fatigue loads. As evident from the experimental results, the shear deformation Δ_c increases with the fatigue cycles due to the fatigue degradation of the CLZ and aggregate interlock. If the deterioration of the CLZ is dominant and V_{CLZ} decreases, the contribution of the other shear mechanisms must increase in order to maintain equilibrium with the applied fatigue load P_{max}. The aggregate interlock contribution V_{ci} will increase due to increased slip displacements in the cracks associated with Δ_c, the stirrup contribution V_s will increase due to the increase of the vertical crack displacements, and V_d will increase due to the increase of the transverse deformation of the bar-dowels. Ultimately, if no fatigue fracture occurs in the transverse and longitudinal reinforcement, it is mainly the smoothening of the cracks and the damage of the CLZ that triggers the shear failure of deep beams.

To comprehensively capture the complex degradation of shear mechanisms and the progressive increase in crack displacements induced by fatigue loading, it is necessary to develop a rational fatigue modeling approach for deep beams. This goal can be achieved within the framework of the two-parameter kinematic theory by updating the constitutive relationships governing each individual mechanism to incorporate fatigue-induced damage. The outcomes of this study, including experimental measurements and analysis, can be used for the development and validation of the 2PKT and other modeling approaches for deep members.

6 | CONCLUSIONS

This paper presented experimental research on five nominally identical deep beams with an a/d ratio of 1.64. Four of the beams were tested under fatigue loading up to failure, while the fifth beam was tested monotonically as a reference specimen. The main testing variables were the maximum and minimum fatigue loads P_{max} and P_{min}. The reference specimen exhibited a shear failure along a critical diagonal crack with crushing of the critical loading zone (CLZ). Through detailed test measurements and analysis, the following main conclusions are reached:

1. Under high maximum fatigue loads (70% of the monotonic strength P_u for beam P4 and 54.7% of P_u for P5), deep beams which are shear critical under monotonic loading are likely to exhibit the same failure mode under repeated fatigue cycles. The global response of such members in terms of mid-span deflection versus the number of fatigue cycles is characterized by three phases: an initial fast increase due to cyclic creep, a slow linear increase, and a rapid increase near failure. This trend is similar to the fatigue behavior of concrete under uniaxial compression.
2. The minimum fatigue load P_{min} has a significant impact on the fatigue life. When P_{min} was increased from 9.7% to 22.5% of P_u (~2.3 times), and P_{max} was kept at 54.7% of P_u, the fatigue life of beam P7 was extended by more than 63 times compared to beam P5.
3. The main fatigue damage of shear-critical deep beams P4, P5, and P7 was the erosion of the surface of the critical shear cracks due to cyclic aggregate interlock, as well as the formation of micro and macro cracks in the critical loading zones (CLZ). Eventually, diagonal crushing of the CLZ under repeated loading triggers the shear failure of deep beams.
4. Despite the pre-cracking in shear of beam P6 at a relatively high load (70% of P_u), the beam with the lowest maximum load (45.1% of P_u) failed in flexure by fatigue fracture of the longitudinal reinforcement. Therefore, a switch of failure modes can be observed from shear to flexure when P_{max} is decreased, and the life of the CLZ is prolonged. Such flexural fractures can be caused by stress concentrators such as tack welds between the longitudinal reinforcement and transverse reinforcement/steel connectors.
5. The two-parameter kinematic model, combined with measurements of vertical displacements in the diagonal cracks, can be used to evaluate the shear deformations and strains in the CLZ of shear-critical deep beams. This model has the potential to provide the basis of a complete modeling approach for crack-based fatigue assessment of deep beams in existing concrete infrastructure.

ACKNOWLEDGMENTS

The project was funded by the Service Public de Wallonie, Belgium, under Belgian Wallonia Research (BEWARE) fellowships according to agreement number 2010240.

DATA AVAILABILITY STATEMENT

The data that support the findings of this study are available from the corresponding author upon reasonable request.

ORCID

Eissa Fathalla https://orcid.org/0000-0002-6284-2567

REFERENCES

1. Comité Euro-International du Béton (CEB) and Fédération Internationale de la Précontrainte (FIP). CEB-FIP model code 1970: final draft. Lausanne, Switzerland: CEB-FIP; 1970.

2. Tilly GP. Fatigue of steel reinforcement bars in concrete: a review. Fatigue Fract Eng Mater Struct. 1979;2(3):251–68.
3. Oudah F, El-Hacha R. Analytical fatigue prediction model of RC beams strengthened in flexure using prestressed FRP reinforcement. Eng Struct. 2013;46:173–83.
4. Zanuy C, Albajar L, De la Fuente P. Sectional analysis of concrete structures under fatigue loading. ACI Struct J. 2009; 106(5):667–77.
5. Fernández Ruiz M, Zanuy C, Natário F, Gallego JM, Albajar L, Muttoni A. Influence of fatigue loading in shear failures of reinforced concrete members without transverse reinforcement. J Adv Concrete Technol. 2015;13(5):263–74.
6. Farghaly SA. Shear design of reinforced concrete beams for static and repeated loads. Doctoral Thesis. Japan: University of Tokyo; 1979 (in Japanese).
7. Higai T. Fundamental study on shear failure of reinforced concrete beams. Proc Jpn Soc Civil Eng (JSCE). 1978;1(279): 113–26.
8. Ueda T. Behavior in shear of reinforced concrete beams under fatigue loading. Doctoral dissertation. Japan: University of Tokyo; 1982.
9. Okamura H, Farghaly SA, Ueda T. Behaviors of reinforced concrete beams with stirrups failing in shear under fatigue loading. Proc Jpn Soc Civil Eng. 1981;308:109–22.
10. Teng S, Ma W, Tan KH, Kong FK. Fatigue tests of reinforced concrete deep beams. Struct Eng. 1998;76(18):347–52.
11. Teng S, Ma W, Wang F. Shear strength of concrete deep beams under fatigue loading. Struct J. 2000;97(4):572–80.
12. Isojeh B, El-Zeghayar M, Vecchio FJ. High-cycle fatigue life prediction of reinforced concrete deep beams. Eng Struct. 2017; 150:12–24.
13. Trandafir AN, Proestos GT, Mihaylov BI. Detailed crack-based assessment of a 4-m deep beam test specimen. Struct Concr. 2023;24(1):756–70.
14. Trandafir AN, Palipana DK, Proestos GT, Mihaylov BI. Framework for crack-based assessment of existing lightly reinforced concrete deep members. ACI Struct J. 2022;119(1):255–66.
15. Aravinthan T, Suntharavadivel TG. Effects of existing shear damage on externally post tensioned repair of bent caps. J Struct Eng. 2007;133(11):1662–9.
16. Mihaylov B, Bentz EC, Collins MP. Two-parameter kinematic theory for shear behavior of deep beams. ACI Struct J. 2013; 110(3):447–55.
17. Mihaylov B. Five-spring model for complete shear behaviour of deep beams. Struct Concr. 2015;16(1):71–83.
18. Zum SV. Verformungsvermögen von Stahlbetonträgern. Ph.D. Thesis. Zürich, Switzerland: ETH Zürich; 1995.
19. Isojeh B, El-Zeghayar M, Vecchio FJ. Concrete damage under fatigue loading in uniaxial compression. ACI Mater J. 2017; 114(2):225–35.
20. Burton KT, Hognestad E. Fatigue tests of reinforcing bars-tack welding of stirrups. ACI J Proc. 1967;64(5):244–52.
21. Helagson T, Hanson JM. Investigation of design factors affecting fatigue strength of reinforcing bars-statistical analysis. Special Publ. 1974;41:107–38.
22. Rehm G, Eligehausen R. Bond of ribbed bars under high cycle repeated loads. ACI J. 1979;76:297–309.

AUTHOR BIOGRAPHIES

Eissa Fathalla, Urban and Environmental Research Unit (UEE), Univ. of Liège, Liège, Belgium.
Email: mmeissa@uliege.be

Boyan Mihaylov, Urban and Environmental Research Unit (UEE), Univ. of Liège, Liège, Belgium.
Email: boyan.mihaylov@uliege.be

How to cite this article: Fathalla E, Mihaylov B. Fatigue behavior of deep concrete beams with critical shear cracks. Structural Concrete. 2023. https://doi.org/10.1002/suco.202300603